Petrography, Chemistry, and Geologic History of Yantarni Volcano, Aleutian Volcanic Arc, Alaska

U.S. GEOLOGICAL SURVEY BULLETIN 1761

Petrography, Chemistry, and Geologic History of Yantarni Volcano, Aleutian Volcanic Arc, Alaska

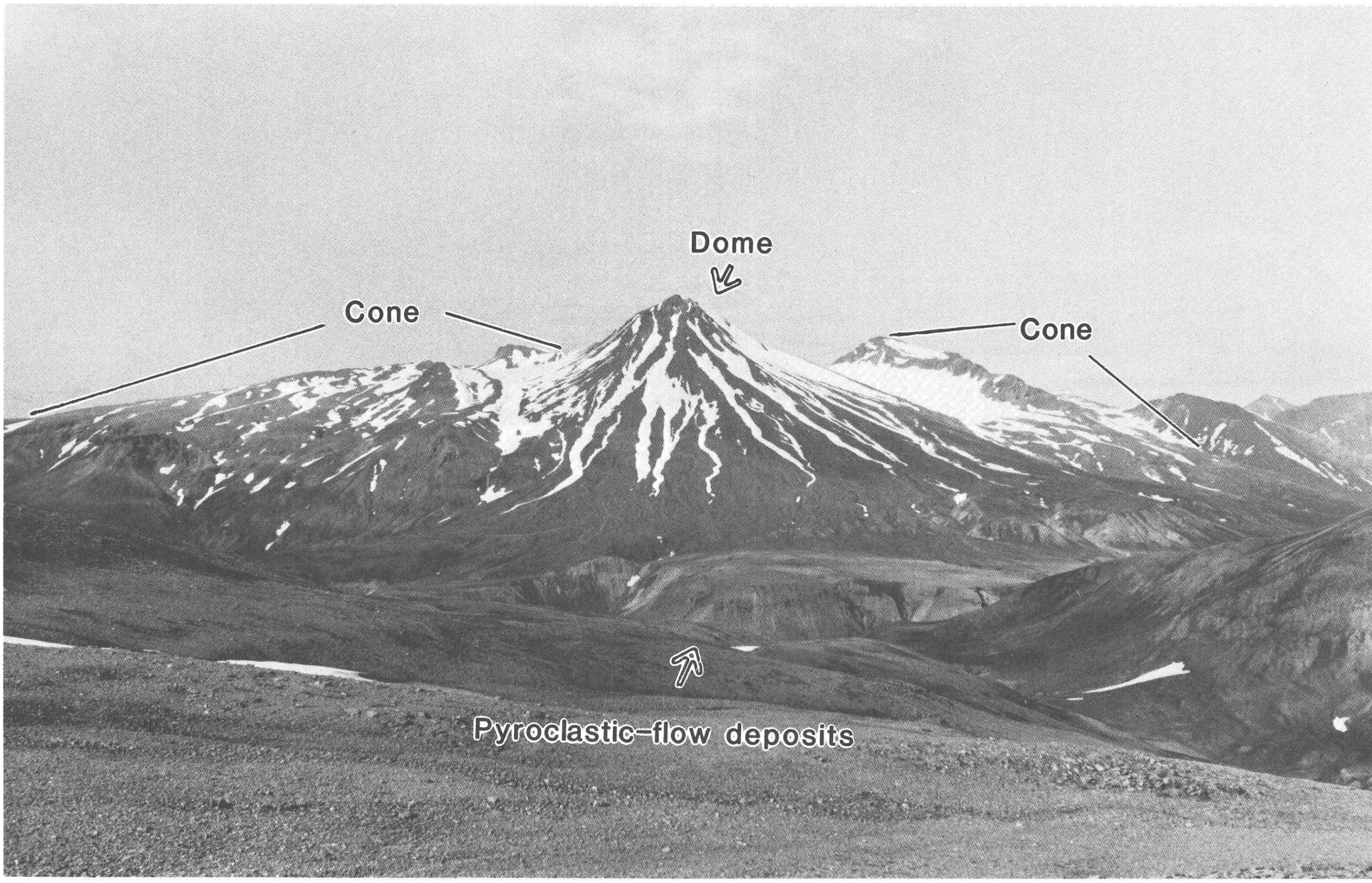

Central dome of Yantarni Volcano, 5 km distant, and flat-topped pyroclastic-flow deposits in middle foreground. View west

Petrography, Chemistry, and Geologic History of Yantarni Volcano, Aleutian Volcanic Arc, Alaska

By J.R. RIEHLE, M.E. YOUNT, and T.P. MILLER

U.S. GEOLOGICAL SURVEY BULLETIN 1761

DEPARTMENT OF THE INTERIOR

DONALD PAUL HODEL, Secretary

U.S. GEOLOGICAL SURVEY

Dallas L. Peck, Director

UNITED STATES GOVERNMENT PRINTING OFFICE, WASHINGTON : 1987

For sale by the
Books and Open-File Reports Section
U.S. Geological Survey
Federal Center, Box 25425
Denver, CO 80225

Library of Congress Cataloging-in-Publication Data

Riehle, J.R.
Petrography, chemistry, and geologic history of Yantarni Volcano, Aleutian volcanic arc, Alaska.

U.S. Geological Survey Bulletin 1761
Bibliography included.
Supt. of Docs. No.: I 19.3:1761
1. Yantarni Volcano (Alaska). 2. Volcanic ash, tuff, etc.—Alaska—Yantarni Volcano region. 3. Geochemistry—Alaska—Yantarni Volcano region. I. Yount, M.E. II. Miller, Thomas P., 1938– . III. Title. IV. Series.
QE75.B9 No. 1761 557.3 s 86–600415
[QE523.Y37] [551.2'1'097984]

CONTENTS

PLATE
[In pocket]

FIGURES

TABLES

Petrography, Chemistry, and Geologic History of Yantarni Volcano, Aleutian Volcanic Arc, Alaska

By J.R. Riehle, M.E. Yount, *and* T.P. Miller

Abstract

Yantarni Volcano is a small (<10 km^3) calc-alkaline center of Quaternary age in the eastern Aleutian volcanic arc 640 km southwest of Anchorage on the Alaska Peninsula. The volcano is composed of andesite and dacite having an SiO_2 range of 55 percent to 63 percent. An ancestral cone consisting of pyroclastic rocks, breccias, and lava flows ranging in composition from two-pyroxene andesite to hornblende dacite began to form at the Yantarni site about 0.46 Ma. Probably between 2,000 and 3,500 years ago, the cone was breached during a catastrophic eruption. The concomitant mass movement of the northeast flank of the cone by a combination of slide and flow resulted in extensive formation of avalanche deposits in the valleys and on ridge slopes northeast of the cone. Emplacement of a dacite dome in the central vent area occurred next, accompanied by block-and-ash flows that filled the valleys and mantled the landslide deposits for distances as great as 6 km east and northeast of the volcano.

Chemical analyses of lithologically representative samples and coexisting phenocrysts suggest that Yantarni magmas are not compatible with closed-system fractionation. Magma mixing, however, is compatible with the chemistry, the petrography, and the occurrence of disequilibrium mineral assemblages.

Yantarni Volcano appears to be a small, intra-segment calc-alkaline center which developed within the past 0.5 m.y. and which has been the site of at least one violent eruption in Holocene time. Violent eruptions of similar character could well occur in the future. Magmas of diverse composition either were erupted in close succession or were mixed shortly before eruption. Yantarni Volcano appears to be in an early stage of development, and a single large magma chamber probably does not exist at shallow depth directly beneath it.

INTRODUCTION AND ACKNOWLEDGMENTS

Yantarni Volcano is a small andesitic stratocone in the eastern Aleutian volcanic arc about 640 km southwest of Anchorage on the central Alaska Peninsula (fig. 1). Eruptive activity at the central vent area began during late Pleistocene time about 0.46 Ma (million years ago) and climaxed with a catastrophic eruption in late Holocene time. The climactic eruption consisted of a debris avalanche followed by emplacement of pyroclastic flows and a dome. Because of the potential for similar future eruptions, a detailed study of Yantarni Volcano was undertaken as part of the Volcano Hazards Program of the U.S. Geological Survey. We present in this report a geologic map, petrographic descriptions, and major-element compositions of representative samples from Yantarni Volcano. From these data, stratigraphic relations, and ^{14}C and K-Ar ages, we infer a geologic history of the volcano.

The region of Yantarni Volcano was mapped in reconnaissance fashion by Burke (1965); later systematic mapping of the region was carried out by Detterman and others (1981, 1983). Initial radiometric dating of volcanic rocks was done by Wilson and others (1981) and Wilson (1982) for purposes of both regional studies and mineral-resource appraisal. Some of these data, cited in this report, help define the age range of magmatism at Yantarni Volcano.

Yantarni Volcano was discovered in 1979 by Robert L. Detterman and James E. Case, and it has had no reported historic eruptions. Neighboring Chiginagak Volcano had reported activity in 1852 and 1959 and Aniakchak in 1931; Veniaminof has been more active, with seven reported eruptions between 1776 and 1950 (Coats, 1950) and eruptions in 1956 and 1983 (Miller, unpublished data).

We gratefully acknowledge Frederic Wilson, who provided three new K-Ar ages and the analytical constants reported in table 3. Judy Hassen and Kathy Egger cheerfully sieved and described most of the samples of pyroclastic deposits for this study; Hassen also provided capable assistance in the field in 1982. Don Richter and Willie Scott provided careful technical reviews which materially improved the manuscript. We also benefited from informal reviews and discussions provided by Fred Barker and Wilson.

GEOLOGIC SETTING

The continental margin lies about 175 km seaward of Yantarni Volcano (fig. 1), and the volcano lies wholly on continental crust. Basement sedimentary rocks in the vicinity of the volcano consist, from oldest to youngest, of continental and marine deposits of Late Jurassic age (Naknek Formation) and Early Cretaceous age (Staniukovich Formation), shallow marine deposits of Late Cretaceous age (Chignik Formation), and continental and marine deposits of early Tertiary age (Tolstoi Formation) (Burk, 1965; Detterman and others, 1983). The southernmost exposures of the Alaska-Aleutian Range batholith are approximately 100 km north of Yantarni Volcano at Becharof Lake (fig. 2) (Reed and Lanphere, 1972). However, batholithic rocks are inferred from magnetic anomalies to extend in the subsurface at least 50 km south of Becharof Lake (Reed and Lanphere, 1973), and an exposure of granitic clasts in Jurassic conglomerate 12 km southwest of Yantarni Volcano implies the presence of granite in the subsurface within 10 to 20 km of the volcano (R.L. Detterman, oral commun., 1985). Surface exposures of a calc-alkaline magmatic arc of Eocene through early Miocene age, termed the Meshik arc by Wilson (1985), are preserved as close as 5 km to the southeast and 8 km to the northwest of Yantarni Volcano.

Yantarni Volcano is colinear with the adjacent Quaternary volcanoes Chiginagak and Kialagvik to the northeast (fig. 2). The Yantarni-Chiginagak-Kialagvik trend lies seaward of an alignment defined by the other Quaternary volcanoes from Veniaminof through Douglas. Alternatively, a single alignment from Veniaminof through Kialagvik can be constructed with Aniakchak lying north of this trend. Such alignments are one means for defining segments of the Aleutian volcanic arc (Fisher and others, 1981; Kay and others, 1982; Kienle and Swanson, 1983), and, depending on how the alignments are defined, Yantarni Volcano may lie near a segment end. Our data that potentially bear on this issue are discussed further in the section "Major-Element and Mineral Compositions of the Volcanic Rocks."

GEOLOGY

Pre-Volcanic Sedimentary Rocks

Pre-volcanic rocks in the area of plate 1 are Upper Jurassic and Lower Cretaceous sandstone, siltstone, and shale (Naknek and Staniukovich Formations, undivided) and Paleocene and Eocene sandstone, conglomerate, and siltstone (Tolstoi Formation) (Detterman and others, 1981, 1983). The Mesozoic rocks are separated from the Cenozoic rocks by a steeply dipping reverse fault that is upthrown on the northwest (pl. 1). The times of movement on the fault within the area of plate 1 are limited to between Paleocene and Quaternary by the ages of displaced strata; there are no data from elsewhere within the region to more closely delimit the timing of movement (R.L. Detterman, oral commun., 1985).

Tertiary Hypabyssal Rocks

The oldest igneous rocks in the immediate vicinity of Yantarni Volcano are dikes, sills, and irregular shallow stocks of late Tertiary age. Their outcrop pattern on plate 1 (slightly modified from Detterman and others, 1981, 1983) shows the occurrence of these hypabyssal rocks for up to 8 km to the south, east, and northwest of Yantarni cone. Two large outcroppings of these rocks 4.5 km southeast of Yantarni Volcano (pl. 1) probably are stocks. Samples of the stocks have about 63 percent SiO_2, indicating a low-silica dacitic composition (samples 50, 54, and 57, table 1).[1] The samples are highly porphyritic and contain xenoliths of hornblende and quartz (table 2). Other exposures northwest of Yantarni Volcano include a felsite sill and areas of hydrothermal activity consisting of altered dikes and wallrocks.

The Tertiary hypabyssal rocks intrude rocks as young as Paleocene and Eocene in age (Detterman and others, 1983). Two samples of hydrothermally altered rocks of the hypabyssal unit (sites 3 and 4, pl. 1) yielded ages of 3.96±0.64 Ma on chlorite (sample 9Yb102; F.H. Wilson, oral commun., 1985) and 3.42±0.28 Ma on plagioclase, 3.48±0.45 Ma on biotite,

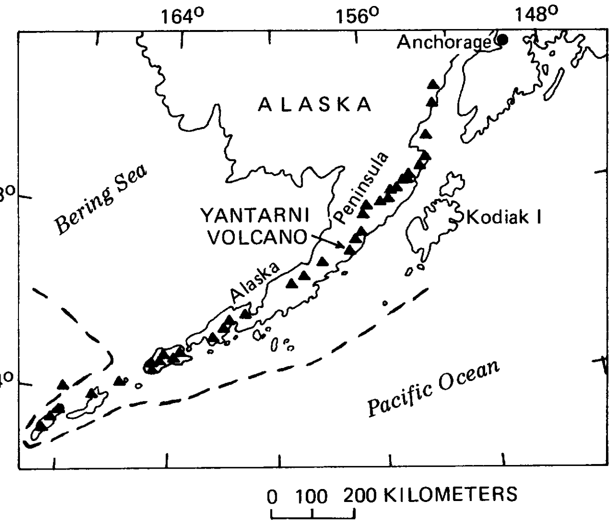

Figure 1. Index map showing location of Yantarni Volcano in eastern part of Aleutian volcanic arc. Dashed line is 200-m isobath, approximate edge of continental crust (Scholl and others, 1975). Quaternary volcanoes are shown as triangles.

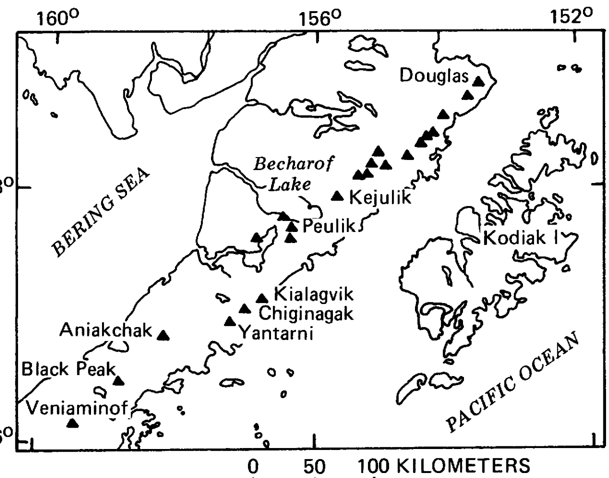

Figure 2. Relation of Yantarni Volcano to adjacent Quaternary volcanoes of Aleutian volcanic arc. In particular, note that alignment of Yantarni, Chiginagak, and Kialagvik Volcanoes lies seaward of alignment defined by volcanoes to northeast and southwest.

---

[1] SiO_2 contents referred to in the text are normalized to 100 percent on a volatile-free basis.

and 2.85±0.17 Ma on chlorite (sample 9Yb101; F.H. Wilson, oral commun., 1985). A sample of the dacitic stock (site 54, pl. 1) yielded an age of 19.3±0.33 Ma on hornblende (sample 9Ws011; Wilson, 1985). The oldest sample is classed with the so-called Meshik volcanic arc (Wilson, 1985), a magmatic arc active from about 40 Ma to 20 Ma. The data are insufficient to permit broad conclusions about temporal patterns of volcanism; however, magmatism at Yantarni Volcano clearly occurred before the current phase of Aleutian volcanism began in late Miocene time (see Marlow and others, 1973).

The preserved volume of rocks assigned to the hypabyssal unit cannot be estimated, owing to the difficulty of distinguishing in detail the irregular contacts of the hypabyssal rocks with adjacent, commonly altered sedimentary rocks.

Older Lava Flows

Moderately to deeply dissected lava flows and associated flow breccias occur as much as 8 km to the southwest, west, and northwest of Yantarni cone (pl. 1). Despite glacial erosion, flow morphology is still apparent in the ridge-top remnants of the early lavas. Topographic knobs within flows of the unit about 6 km southwest of the cone may be vent plugs (pl. 1).

The lava flows are porphyritic, locally trachytic, two-pyroxene andesites (table 1) with fine-grained or microcrystalline groundmass (table 2). The degree of alteration varies from sample to sample; the most altered rocks have propylitic alteration assemblages including some or all of chlorite, quartz, iron oxide, and uncommon white and brown mica, whereas other samples have glass in the groundmass (table 2). However, we know of no samples or outcrops of older lava flows that are bleached to the bright white, red, or yellow shades typical of fumarolic alteration.

The older lava flows are not in contact with the Tertiary hypabyssal rocks within the area of plate 1. One K-Ar determination of an older lava flow yielded an age of 0.47±.05 Ma (sample 24, table 3) and a previous whole-rock determination yielded one of 0.62±0.23 Ma (site 30, pl. 1; sample 8Dt034, Wilson and others, 1981). We consider an implied age range of

Table 1. Major-element whole-rock analyses of Yantarni samples

[Analysts: A.J. Bartel, S. Neil, K. Stewart, L. Espos, J. Taggart, S. Roof, and E. Brandt, U.S. Geological Survey. Methods: X-ray fluorescence for all except FeO, which is titration]

	Hypabyssal rocks			Older lava flows							Cone-building deposits					
	50	57	54	26	24	29	1a	1b	2	25	33	16	17	19	48	32
SiO_2	60.2	61.6	63.5[1]	59.4	55.9	55.5	58.6	57.5	56.4	55.9	62.6	58.6	57.4	56.9	59.2	62.5
TiO_2	.64	.64	.71	.76	.80	.88	.97	.85	.83	.87	.66	.78	.84	.85	.91	.68
Al_2O_3	16.0	16.3	15.6	17.2	16.4	16.8	16.5	16.4	16.1	16.4	16.7	17.1	17.6	17.3	17.2	16.8
Fe_2O_3	1.98	2.68	3.14	3.27	4.42	3.40	3.04	3.24	5.29	4.12	2.18	3.38	3.68	3.00	5.70	3.25
FeO	2.99	2.32	1.82	3.40	3.05	4.14	4.47	4.45	2.22	4.21	3.27	3.58	3.87	4.39	1.55	2.40
MnO	.09	.06	.07	.14	.13	.14	.15	.15	.14	.14	.12	.13	.13	.14	.14	.12
MgO	3.35	3.10	2.68	2.90	3.82	4.46	4.08	4.43	3.85	4.18	2.42	3.27	3.77	4.10	3.19	2.53
CaO	4.70	5.17	4.45	7.28	8.04	7.72	7.78	8.18	7.68	8.43	6.00	7.45	7.80	8.20	6.77	5.82
Na_2O	3.54	3.77	3.68	2.81	2.76	2.46	2.71	2.83	2.56	2.73	3.04	2.76	2.69	2.78	2.90	3.24
K_2O	1.66	1.52	2.16	1.37	1.47	1.26	1.49	1.64	1.51	1.66	1.55	1.37	1.26	1.37	1.36	1.53
P_2O_5	.19	.22	.12	.14	.19	.18	.18	.22	.17	.24	.16	.13	.16	.16	.18	.16
LOI[2]	4.38	2.48	2.73	1.44	2.88	3.22	.53	.49	3.33	.66	1.13	1.24	.99	.89	1.00	.95
Total	99.7	99.9	100.7	100.1	99.9	100.2	100.5	100.4	100.1	99.5	99.8	99.8	100.2	100.1	100.1	100.0

	Cone-building deposits--Continued								Holocene pyroclastic-flow deposits						Dome	
	35	20	46	36	41	34	31	44	11b	11c	11d	11e	12	7	39	38
SiO_2	60.6	58.0	57.5	57.3	62.1	61.3	60.2	59.4	55.0	60.1	63.1	60.6	60.8	60.0	61.1	60.4
TiO_2	.80	.83	.81	.77	.75	.71	.78	.85	.93	.75	.64	.73	.75	.70	.72	.72
Al_2O_3	17.1	17.2	17.3	17.4	16.7	17.0	16.9	17.1	17.4	16.8	16.4	16.7	16.6	16.3	16.7	16.8
Fe_2O_3	4.07	2.80	3.58	3.19	2.49	2.45	4.90	2.83	3.65	3.78	2.84	3.58	3.04	4.84	2.67	2.74
FeO	2.13	4.31	3.81	4.10	3.46	2.61	1.10	3.95	4.54	2.62	2.36	2.74	3.34	.89	3.42	3.52
MnO	.12	.14	.13	.18	.13	.11	.04	.13	.14	.12	.31	.13	.13	.05	.12	.13
MgO	2.69	3.87	3.48	3.76	2.52	2.87	2.21	3.00	4.50	3.21	2.41	3.08	3.15	2.71	2.93	3.28
CaO	6.01	7.76	8.10	7.83	6.01	6.30	5.02	6.71	9.12	7.25	6.00	6.92	6.85	4.80	6.81	7.21
Na_2O	2.91	2.99	2.89	2.76	2.92	3.08	2.92	2.70	2.46	2.73	2.98	2.81	2.96	2.72	2.82	2.78
K_2O	1.24	1.46	1.43	1.25	1.53	1.48	1.43	1.22	1.29	1.64	1.80	1.58	1.64	1.41	1.64	1.58
P_2O_5	.17	.17	.17	.13	.16	.17	.16	.17	.15	.17	.15	.14	.15	.18	.15	.16
LOI[2]	1.91	.88	1.11	1.20	.87	1.12	3.84	1.15	1.11	.83	.75	1.00	.55	5.34	.90	.39
Total	99.8	100.4	100.3	99.9	99.6	99.2	99.5	99.2	100.3	100.0	99.7	100.0	100.0	99.9	100.0	99.7

[1] Analysis from F.H. Wilson (oral commun., 1985).

[2] Loss on ignition to 925 °C for 40 minutes. Value reported here has been corrected for oxidation of FeO to Fe_2O_3 and should include only volatiles.

Table 2. Petrographic descriptions of Yantarni samples

[Abbreviations are as follows: apat, apatite; calc, calcite; chlor, chlorite; cpx, clinopyroxene; gndms, groundmass; hbl, hornblende; hem, hematite; lith, lithic; oliv, olivine; opaq, opaque; opx, orthopyroxene; plag, plagioclase; px, pyroxene; qtz, quartz; tr., trace]

Sample	Textures	Alteration	Modal phenocrysts								
			Plag	Cpx	Opx	Hbl	Qtz	Oliv	Opaq	Gndm	Lith
		Tertiary hypabyssal rocks (unit Ti)									
50	Porphyry; gndms <0.1 mm, massive, plag>>chlor=mica; qtz as anhedral mosaics (xenoliths); apat microphenocrysts	Plag altered to chlor/mica, hbl to chlor/hem; veinlets of hem/calc/mica	18.0	(altered px 4.8 percent)		3.0	5.5	0	0.7	67.7	0
54[1]	Porphyry; gndms <0.1 mm, massive, plag>>hbl>opaq=apat; qtz as anhedral mosaics (xenoliths); plag fractured and recrystallized?	Rare calc and chlor as replacement of mafics in lithics	15.7	0	0	9.4	1.2	0	.2	69.5	4.2
57	Porphyry; gndms <0.1 mm, massive, plag>hbl>opaq; qtz phenocrysts embayed and rounded; rare euhedral apat microphenocrysts	Hbl altered to chlor/opaq/px	15.8	0	0	12.1	1.1	0	.8	70.1[2]	0
		Older lava flows (unit Qof)									
1	Porphyry; gndms very fine grained felted mat of plag needles, px and opaq grains	Rare hem	22.7	9.5	7.4	0	.6	0	3.1	56.7	0
1B	Porphyry; gndms <0.1 mm, plag>px=opaq	Rare hem	21.7	11.4	3.4	0	0	0	2.7	60.8	0
2	Porphyry; gndms <.05 mm, plag/opaq/px	Chlor/hem alteration of gndms and opx	28.8	7.6	4.5	0	0	0	2.9	55.6	.4
24	Porphyry; gndms <0.1 mm, plag>>chlor+mica>cpx=opaq; cpx rims on opx phenocrysts; originally vitric?	Zeol/calc/chlor+mica as vugs in gndms and as replacement of px phenocrysts and lith	19.2	4.5	3.0	0	0	0	1.2	70.3	1.8
26	Devitrified vitrophyre; gndms <0.3 mm, massive, microcrystalline; rare fine-grained lith	Trace chlor/calc/zeol as alteration of gndms and plag	33.6	5.4	4.2	0	0	0	3.0	53.8	.2
28	Porphyry; gndms microcrystalline plag and secondary patches of chlor+mica	Mafics and gndms altered to hem/calc/chlor/mica/zeol	24.6	(altered px 10.0 percent)		0	0	0	1.2	63.2	1.0
29	Vitrophyre; gndms <0.2 mm, plag>>cpx=opaq>glass; rare reacted hbl; cpx rims on some opx phenocrysts	None	20.3	5.0	3.8	0.2	0	0	1.3	66.8	3.0
		Cone-building deposits (unit Qyc)									
16	Porphyry; gndms <0.1 mm, plag microlites and rare glass; seriate phenocrysts	None	30.7	8.0	4.0	0	0	0	2.3	55.0	0
17	Porphyry; gndms microcrystalline, rare glass; phenocrysts 0.1-2 mm; microphenocrysts of plag≥opx=cpx>opaq	None	24.2	3.7	2.8	0	0	0	1.3	67.7	.3
18	Porphyry; gndms microcrystalline to 0.3 mm, vaguely foliated plag>>cpx=opx=opaq; qtz rimmed by cpx; microvesicular	None	16.2	1.5	2.5	0	tr.	.8	.7	73.5	4.8
19	Porphyry; gndms microcrystalline to 0.2 mm, foliated plag>>cpx=opaq>opx	None	19.6	3.3	3.9	0	0	1.4	1.8	70.1	0
20	Porphyry; gndms <0.01 mm, px>plag>opaq; plag/cpx/opaq microphenocrysts	None	22.3	4.6	4.1	0	0	1.3	1.7	63.9	1.7
21	Porphyry; gndms <0.1 mm, plag>px>opaq; cpx overgrowths on opx grains	Hem alteration of opx and as fracture filling	31.4	3.9	8.0	0	0	0	2.0	54.8	0
22	Porphyry; gndms anhedral mosaic of secondary quartz	Intensely altered; phenocryst pseudomorphs of calc/zeol/chlor	-	-	-	-	-	-	-	-	-
33	Vitrophyre; plag microlites in glass; phenocrysts 0.2-5 mm; hbl fresh, some intergrown with px	None	28.3	2.8	4.4	.4	0	0	1.6	62.2	.3
34	Devitrified vitrophyre? gndms massive, microcrystalline plag>cpx>opx=opaq;seriate phenocrysts >0.2 mm; rare oxidized hbl	Rare zeolites in gndms	21.8	3.1	1.6	tr.	0	0	1.6	71.1[3]	1.0
35	Porphyry; gndms <0.1 mm, foliated plag>chlor/mica>opaq; phenocrysts seriate to 3 mm; diabasic lithics	Mafics altered to calc, chlor/mica, opaq	28.0	.2	0	0	0	0	1.5	61.0[4]	9.7

Table 2. Petrographic descriptions of Yantarni samples--Continued

Sample	Textures	Alteration	Modal Phenocrysts Plag	Cpx	Opx	Hbl	Qtz	Oliv	Opaq	Gndms	Lith
		Cone-building deposits--Continued									
36	Porphyry; gndms <0.1 mm, plag>opaq> px	Opx altered to chlor/ hem	32.9	3.6	5.9	0	0	0	2.6	52.5	2.3
40	Porphyry; gndms microcrystalline, massive; both plag and gndms fractured placed	Gndms and plag veined and replaced by isotropic material	22.2	1.0	2.7	1.7	.3	0	.8	70.3	1.0
41	Porphyry; gndms <0.1 mm, massive and microcrystalline; microphenocrysts of plag>>cpx>opx=hbl; phenocrysts to 2 mm; hbl heavily oxidized	Zeolites in gndms	21.2	2.0	5.3	.3	0	0	1.8	62.0	7.3
42	Devitrified vitrophyre? Gndms microcrystalline plag; bimodal phenocrysts to 2 mm; diabasic and pyroxenitic lithics	None	23.0	1.2	2.2	.7	0	0	2.0	68.2	2.8
44	Porphyry; hyalopilitic; gndms <0.1 mm, plag>glass>px>opaq	None	36.6	3.0	4.4	tr.	0	0	2.6	51.6	1.8
46	Porphyry; gndms <0.1 mm, mottled appearance due to variation in proportion of light and dark minerals	Sparse hematite	27.3	5.5	5.2	0	0	0	.8	59.2	2.1
47	Porphyry; gndms <0.05 mm, plag>opaq =px	Sparse hem alteration of plag and gndms	24.9	7.9	5.3	0	0	0	2.2	59.8	0
48	Porphyry; gndms microcrystalline, locally foliated; phenocrysts >0.2 mm; rare, heavily oxidized hbl; diabasic lithics	Oxidized rims on opx, hbl nearly totally oxidized; gndms recrystallized opaqs	29.5	.5	4.2	tr.	0	0	2.0	60.3	3.5
52	Porphyry; gndms microcrystalline, massive; phenocrysts >0.5mm	Phenocrysts heavily altered to clay and hem; gndms recrystallized	25.0	.5	1.0	tr.	.2	0	.5	70.3[5]	2.7
		Holocene pyroclastic-flow deposits (unit Qp) and dome (unit Qdy)									
11b	Vesicular vitrophyre; gndms 0.2-0.4 mm, plag>cpx=hbl>opaq(opx?); hbl rimmed by cpx and plag; rare glass	None	10.3	.3	.5	.7	0	0	.3	87.8	0
11c	Vitrophyre; gndms <0.2 mm, foliated plag>cpx>opaq; cpx as microphenocrysts or rims on qtz; hbl reacting to px/ plag/opaq	None	19.0	.3	1.2	1.0	.3	0	1.8	73.5	2.8
11d	Vitrophyre; gndms <0.2 mm, foliated plag>cpx>opaq; microvesicular; hbl reacted and oxidized	None	22.7	.8	2.0	2.8	.7	.2	1.3	69.2	.3
13	Porphyry; gndms <0.2 mm, massive plag>px>opaq; cpx only as microphenocrysts; hbl reacted and oxidized	Gndms recrystallized and replaced by opaq; zeolitized lith	19.4	.4	3.4	4.0	1.2	0	tr.	68.8	2.8
14	Devitrified vitrophyre? Gndms microcrystalline, foliated plag>>cpx= hbl=opx=opaq; cpx only as microphenocrysts; bimodal phenocryst sizes	None	23.3	.2	1.5	5.0	1.2	0	.8	67.6	.3
38	Porphyry; gndms <0.1 mm, foliated plag>opx=hbl=opaq; phenocrysts bimodal, 0.1 to 3 mm; hbl reacting to plag/cpx/opaq	None	19.8	.8	2.2	1.0	.8	0	.8	72.0	2.5
39	Porphyry; gndms <0.2mm, vague foliation, plag>cpx>hbl=opx=opaq; thin oxide rims on hbl, cpx rims on qtz	None	28.2	.2	2.5	2.3	1.3	.2	2.2	62.8	.3

[1] Description modified from F.H. Wilson (oral commun., 1985) for inclusion here.
[2] Includes 10.5 percent alteration pseudomorphs, formerly hornblende(?) microphenocrysts.
[3] Modes here are exclusive of a single large lithic clast consisting of porphyritic diabase.
[4] Includes 6.8 percent alteration pseudomorphs, formerly mafic phenocrysts.
[5] Includes 7.5 percent alteration pseudomorphs, formerly mafic(?) phenocrysts.

middle to late Pleistocene to be consistent with the moderate degree of glacial erosion of these rocks.

We estimate the preserved volume of older lava flows to be 0.60 km^3. The original volume of the rocks making up the unit is difficult to assess because glacial erosion has clearly removed some material. The present distribution of flows on ridges, however, suggests topographic inversion. In such a case the flows would initially have been confined to topographic lows rather than spread out as broad plateaus, and the original volume would probably have been no more than two or three times the preserved volume.

Lava Flows, Breccias, and Older Pyroclastic Deposits of Yantarni Cone

Deposits of this unit compose Yantarni cone, a physiographic feature moderately dissected by glacial erosion. The basal cone deposits on the north flank are pyroclastic rocks that lie unconformably on rocks of the Jurassic Naknek Formation; they are composed of monolithologic, slightly vesicular cobble- to boulder-sized clasts with a small amount of fine-grained matrix. An SiO_2 content of 59 percent from a single clast (sample 16, table 1) indicates an andesitic composition. The deposit, probably the result of dome collapse, is included in the cone-building unit rather than the older lava flows because its pyroclastic nature indicates central-vent volcanism.

The basal deposit on the east side of the cone is an andesitic lava flow approximately 50 m thick (sample 46, table 1) which may belong to the unit of older lava flows. It is overlain, however, by a thick succession of volcaniclastic deposits that we assign to the cone-building unit, and owing to the insignificant outcrop area of the lava flow we have included it within the cone-building unit.

Coarse breccias, some brightly colored by fumarolic alteration, and interbedded lava flows make up the basal cone deposits on the southwest side of the cone. The breccias can be traced laterally to an origin high on Yantarni cone, and the contact with the unit of older lava flows (pl. 1) is arbitrarily placed at the base of the oldest breccia. On the west side of the cone, breccia rests directly on pre-volcanic sedimentary rocks.

Samples of the cone-building unit range widely in composition, from two-pyroxene andesite to hornblende-bearing dacite (tables 1 and 2), and include fresh, glassy lavas as well as yellow to orange, fumarolically altered varieties in the breccias. One of the lowest SiO_2 contents of the sample set (57 percent; sample 19, tables 1 and 2), as well as some of the highest (62-63 percent; samples 31, 32, 33, 34, and 41, tables 1 and 2), occur in lava flows stratigraphically high on the southeast rim of the crater and on the south flank of the volcano. There is no apparent relation between composition and stratigraphic position in the cone-building unit.

A sample of the basal cone deposits on the north side of the cone yielded a K-Ar age of 0.46±0.12 Ma (sample 77, table 3), thus the onset of the cone-building phase of volcanism overlaps or closely succeeds the closing stages of early lava-flow activity. Another sample of a lava flow stratigraphically high in the cone-building deposits yielded an age of 0.41±0.09 Ma (sample 19, table 3). The cone retains the outline of its original form (see frontispiece) but is incised in all quadrants by glacially eroded valleys, and we infer that cone construction was largely completed before late Pleistocene glaciation. The inference is consistent with the youngest radiometric age of the sample that is stratigraphically high in the cone-building unit (0.41 Ma; sample 19).

We estimate the present volume of the cone--that is, of this unit--to be about 2.7 km^3. The volume of debris-avalanche deposits (discussed later) is about 0.8 km^3; most of that material was originally part of

Table 3. Radiometric-age determinations of Yantarni samples

[Analysts: Argon and age calculation, F.H. Wilson, N. Shew, and G.D. DuBois; potassium, S. Neil. Data provided by F.H. Wilson]

Sample	Mineral dated	K_2O (wt pct)	$^{40}Ar_{rad}$ (mol/gx10^{-12})	$^{40}Ar_{rad}$ (pct)	Age (Ma)
77	Plagioclase	0.277; 0.276	0.21163	3.6	0.542±0.038
		.267; .265	.14837	1.7	.380±0.019
		avg .271		avg	0.461±0.122
19	Plagioclase	.348; .341	.17799	4.8	.357±0.042
		.357; .340	.23018	4.9	.461±0.027
		avg .349		avg	0.409±0.089
24	Whole rock	1.499; 1.490	.95619	12.4	.444±0.009
			1.0553	3.2	.490±0.041
		avg 1.495		avg	0.467±0.053

λ_ε = 0.572x10^{-10} yr^{-1}; λ_β = 4.962x10^{-10} yr^{-1}; $\lambda_{\varepsilon'}$ = 8.78x10^{-13}yr^{-1};

$^{40}K/K$ = 1.167x10^{-4}mol/mol

the cone-building unit, and before the avalanche the volume of the cone must have been about 3.5 km^3. The maximum volume of the cone before glacial erosion is roughly estimated to be 6.6 km^3 by assuming a smooth cone of 5.6 km diameter and 0.8 km height.

Debris-Avalanche Deposits, Younger Pyroclastic Flows, and Dome

The four youngest mappable deposits of Yantarni Volcano are avalanche debris consisting of blocks of altered cone material (two units), pyroclastic-flow deposits, and a dome (pl. 1). These deposits, which have the unifying aspect of being unmodified by glacial erosion, are discussed together because we infer that the deposits are partly contemporaneous in age and have related origins. The debris-avalanche deposits are largely covered by the succeeding pyroclastic-flow deposits, and by inspection of the geologic map we estimate that their volume is about one-half that of the pyroclastic-flow deposits. Also by inspection, we approximate the dome by a cylinder 1 km in diameter and 300 m high. From such assumptions, we estimate the total volume of avalanche material (both units) as 0.8 km^3, of pyroclastic-flow deposits as 1.0 km^3, and of the dome as 0.25 km^3.

Debris-avalanche deposits

Deposits from debris avalanches form two separate mappable bodies, one northeast and one south of Yantarni Volcano. The northeastern avalanche deposits (map unit Qda, pl. 1) resulted from a major catastrophic mass movement of the northeast part of Yantarni cone. As is typical of such deposits elsewhere, combinations of slide and flow were involved in their emplacement, and the distribution of the deposits is strongly dependent on the local topography. The deposits are composed of a chaotic assemblage of material that originally occupied the northeast part of the cone, now the open part of the U-shaped amphitheater surrounding Yantarni dome (pl. 1). This material has a distinctive orange-brown color and a bleached appearance and is presumed to have originally been strongly altered and oxidized coarse breccia and volcaniclastic rocks of the cone-building unit. Boulders of native sulfur as large as a meter in diameter are found locally near the base of the deposits, and much of the altered material is pyritiferous. The deposits show a large range in sorting, from coherent masses as large as several hundred meters across to disaggregated, matrix-rich material with clasts no larger than lapilli size.

The avalanche deposits are exposed chiefly on valley flanks and floors northeast of the volcano (pl. 1). Their total extent, however, is much greater than that shown on the geologic map because they are generally covered by the younger pyroclastic-flow deposits, which conceal much of the original surface and characteristic hummocky topography of the avalanche deposits. Avalanche blocks are locally caught up in the overlying pyroclastic-flow deposits (fig. 3).

Immediately northeast of Yantarni dome, the avalanche mass apparently slid or moved as a coherent block. The block forms a low terrace 100 m high (fig. 4), which extends about 3 km in a northwest-southeast direction and is overlain by a thin veneer of block-and-ash-flow deposits. At least some original bedding and structure is preserved in spite of estimated movement from its point of origin of 1-2 km horizontally to the northeast and 300-400 m vertically.

Farther downslope to the northeast, however, the avalanche mass apparently disaggregated and became much more mobile. The avalanche had sufficient momentum that on reaching the southwest-facing ridge of older rocks northeast of the creek, it moved up the ridge to an elevation of at least 550 m (1,800 ft) above sea level, or 335 m (1,100 ft) above the present valley floor (pl. 1). Deposits of altered and oxidized cone material from the avalanche are plastered across this slope (fig. 5). The highest point on this ridge, which must have been directly in the path of the avalanche, is about 850 m (2,800 ft) above sea level, and the avalanche, which at that point was probably behaving like a flow, does not appear to have surmounted this barrier. The ridge axis slopes down to the southeast to an elevation of 460 m (1,500 ft) above sea level within a kilometer, but no avalanche deposits are found on or northeast of the ridge. The axis of the avalanche movement, therefore, as defined by the thickest and highest deposition of material, is N. 45° E. of the volcano.

The scattered avalanche deposits of the northeastern unit form the basal part of deposits of the most recent significant activity at Yantarni Volcano. We infer that at least some of the overlying pyroclastic flows were emplaced simultaneously with the avalanche, as blocks of cone material are in the pyroclastic-flow deposits (figs. 3 and 7). Our inference is based on the assumption that the pyroclastic flows did not erode large blocks of material, but the pyroclastic flows instead were intimately mixed with blocks in the trailing part of the avalanche. Such evidence, however, does not unequivocally preclude the possibility of a hiatus measured in years between the avalanche and the pyroclastic flows.

The southern avalanche deposit (map unit Ql, pl. 1) consists of a poorly sorted deposit of blocks, some several meters in diameter, in the glaciated valley on the south side of the cone. The deposit does not appear to be a catastrophic landslide because the toe of the deposit is confined to the valley floor and does not run up the opposing (south) valley wall where the valley bends (fig. 6). A lava flow at the west margin of the deposit near the bend has been beheaded, and we infer that the lava flow was emplaced on a glacier that now is largely wasted. Other, permissive evidence for subsurface ice includes a hummocky surface and springs at the toe of the deposit. Steep lateral margins and subarcuate ridges in the deposit suggest slow, possibly continuing movement of a landslide or rock glacier (R.W. Fleming, oral commun., 1982), a mechanism consistent with initial deposition on glacial ice. The deposit is remarkable, however, for both its thickness and the size of its largest clasts, and we conclude that the deposit has a more complex history than a simple surface moraine or rock glacier. We infer that the deposit probably originated in limited mass movement of cone material onto glacier ice during the catastrophic eruption. By analogy to

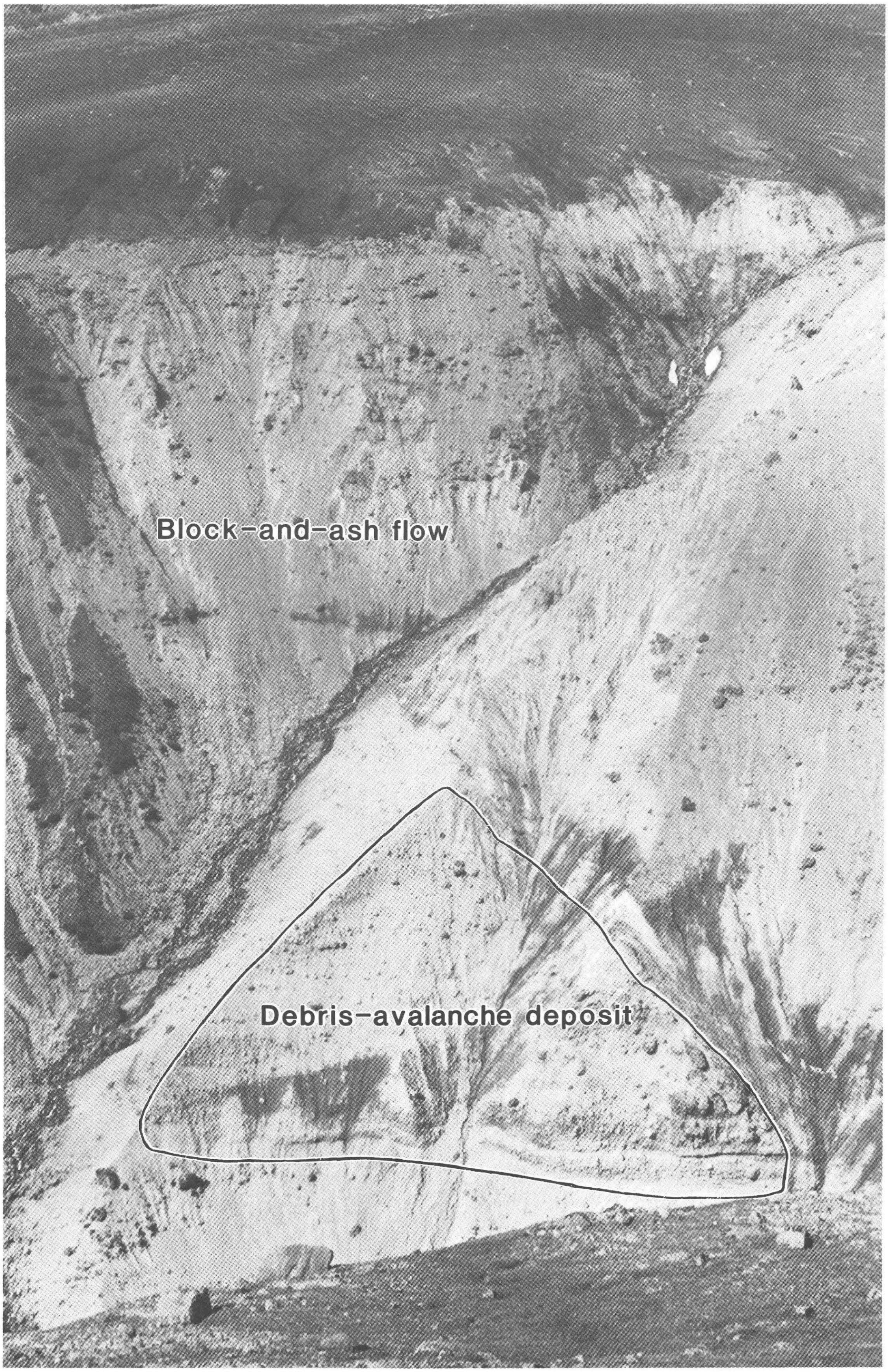

Figure 3. Debris-avalanche block caught up in block-and-ash flow, east side of Yantarni Volcano. Height of exposure about 50 m.

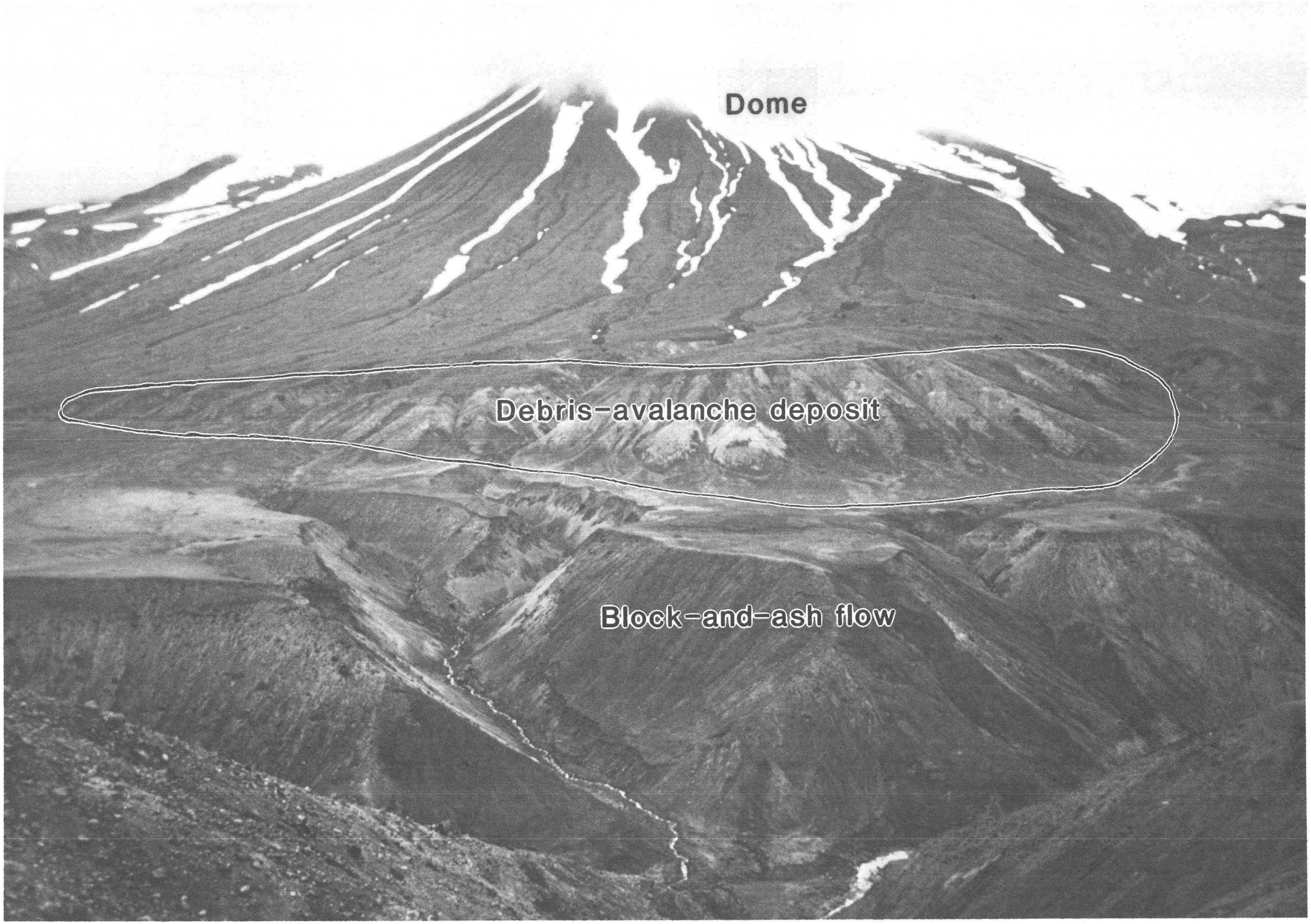

Figure 4. Flat-topped pyroclastic-flow deposits in foreground, terracelike coherent debris-avalanche deposit in center, and base of central dome of Yantarni Volcano in background. View southwest.

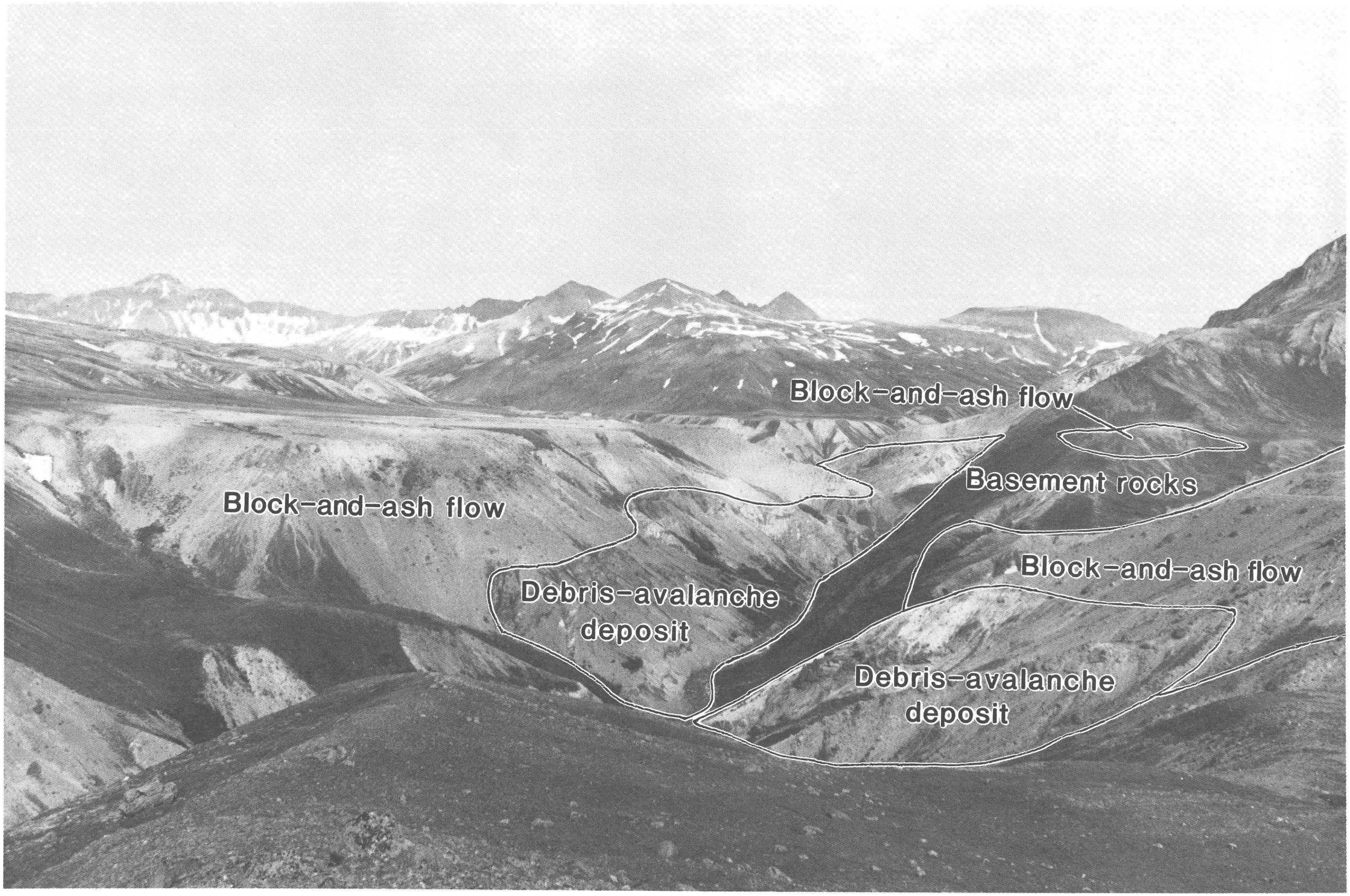

Figure 5. Valley-fill debris-avalanche deposits underlying pyroclastic flows (center) and mantling basement-rock slopes to right. Area is 4 km northeast of central dome of Yantarni Volcano. View northwest.

Shoestring Glacier at Mount St. Helens (Brugman and Meier, 1981), wasting of ice was probably a response mainly to beheading rather than to erosion and melting during emplacement of cone material.

Younger pyroclastic-flow deposits

The undifferentiated, younger pyroclastic-flow deposits and talus of the dome compose a fan-shaped apron that extends northeast from the dome and partly fills the valley of the adjacent creek (pl. 1). Generalized sections measured in the deposits at three localities are shown on figure 7. The upstream section (site 14, pl. 1) consists of a monolithologic deposit of slightly vesicular, subrounded blocks of red-brown lava in an ash matrix which ranges from less than 10 percent by volume at the base to as much as 25 percent at the top. A single sample (14, table 2) closely resembles samples of the dome (samples 30 and 38, table 2) in both texture and modal phenocryst content. The middle section (site 11, fig. 7B) consists of several pyroclastic-flow deposits, ranging from a poorly sorted, fine-grained base on the avalanche deposits to a top consisting of moderately sorted beds of slightly vesicular lapilli and blocks of lava. The downstream section (site 55, fig. 7C) consists of a single bed of lava blocks that overlies a bed of poorly sorted fine-grained tuff, which in turn overlies avalanche deposits.

The lower pyroclastic-flow deposits of the middle section (samples 11b and 11e, fig. 7) have 50 percent or more ash matrix, and on the basis of their granulometry (fig. 8) we classify them as ash-flow tuffs. The analyzed samples are, of course, representative only of the fine-grained matrix. The blocks shown on each stratigraphic section may be lag

Figure 6. Stereopair showing deposit of mass movement on southeast flank of Yantarni Volcano. Deposit is interpreted to have covered glacial ice, now largely melted, and to have originated in limited mass movement during cone-destroying eruption. Deposit is not the result of catastrophic debris avalanche because it does not run up south wall of valley at curve.

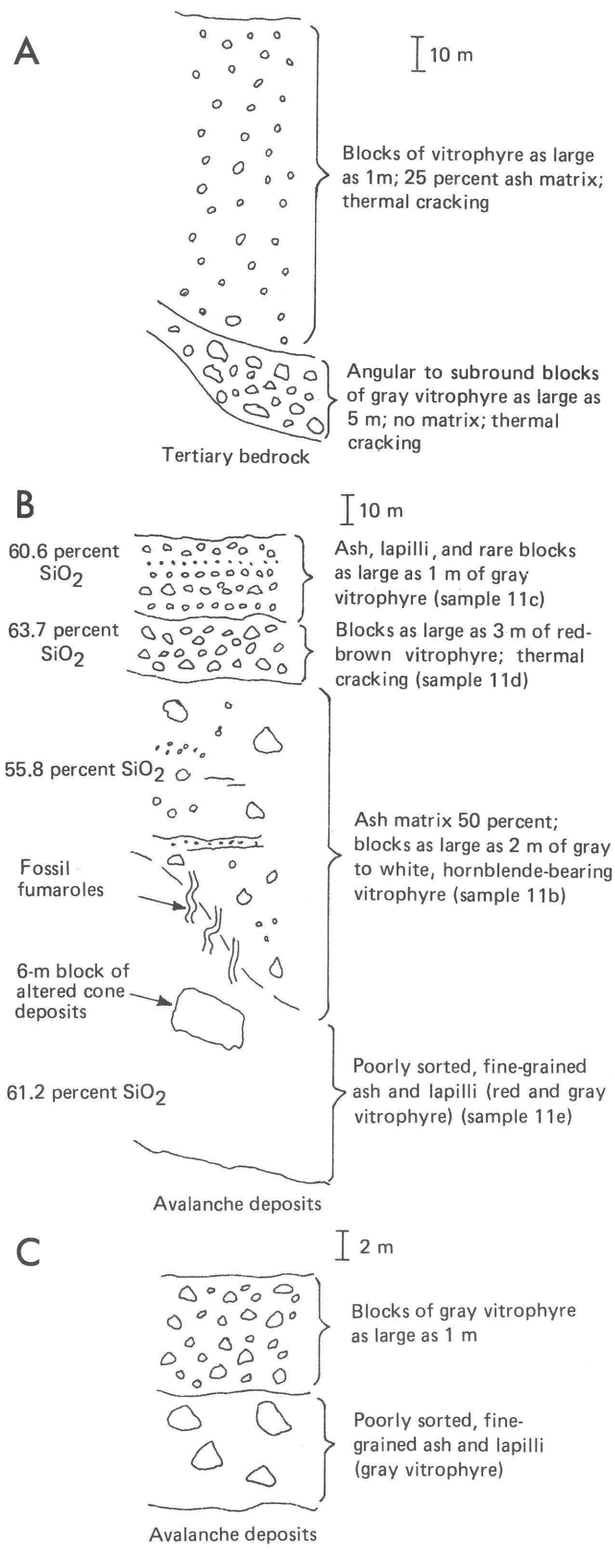

Figure 7. Measured sections in pyroclastic-flow deposits (see pl. 1 for locations). A, Site 14. B, Site 11. Petrographic details and grain-size distributions provided in figure 8. C, Site 55.

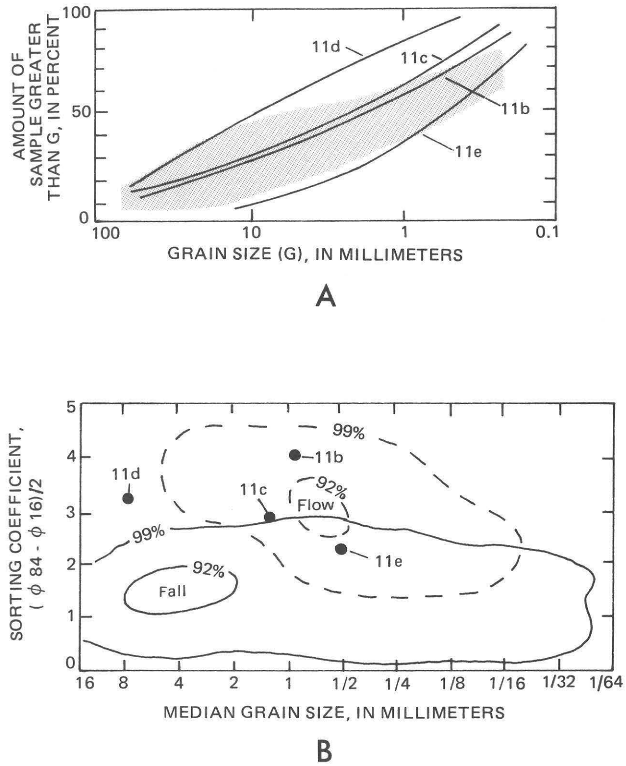

EXPLANATION

Megascopic petrographic descriptions of large juvenile clasts from site 11 (pl. 1)--see table 2 for descriptions from microscopic examination. plag, plagioclase; hbl, hornblende; px, pyroxene

11b Porphyry or vitrophyre, pale gray, slightly vesicular or diktytaxitic; large phenocrysts of plag > hbl=px

11c Porphyry or vitrophyre, pale to medium gray, slightly vesicular; large phenocrysts of plag > hbl=px; rare altered porphyry

11d Porphyry or vitrophyre, red-brown groundmass, slightly vesicular; phenocrysts of plag > px=hbl; trace agglutinated(?) scoria

11e Vitrophyre, red brown and pale gray, slightly diktytaxitic, hbl-bearing

Figure 8. Granulometric data for Yantarni pyroclastic-flow deposits. A, Grain-size distributions of matrix samples. Shaded area includes cumulative curves for several pyroclastic-flow deposits of Mount St. Helens (Kuntz and others, 1981). B, Median size versus sorting coefficients. Fields encompassing 92 and 99 percent of pyroclastic-flow and pyroclastic-fall samples of Walker (1971) are shown.

breccias formed by the selective removal of finer material during pyroclastic flow (Wright and Walker, 1977). Such deposits were observed to form in several environments at Mount St. Helens (Rowley and others, 1981), such as along the margins of pyroclastic flows, on steep underlying slopes, or at changes in the gradient of the underlying slope. However, the prominent occurrence of blocks as a single bed at the sites of all three measured sections implies that the blocks are more representative of a single depositional event than of subtle facies changes within numerous depositional units. Consequently, we interpret the blocks to be the deposit of one or more block-and-ash flows of the Merapi type (Williams and McBirney, 1979, p. 152-154), a deposit that originated in relatively nonexplosive collapse of a dome at Yantarni that developed after the avalanche of debris.

Evidence that the pyroclastic-flow deposits were emplaced at high temperatures includes fossil fumarole pipes in the lower ash-flow tuffs and spalled or intricately cracked blocks and breadcrust bombs in the uppermost beds (fig. 9). The SiO_2 contents of four juvenile clasts from the deposits (samples 11b, 11c, 11d, and 11e; table 1) are from 55.7 percent to 63.7 percent, the lowest and highest silica contents of the sample set. The highest SiO_2 content (sample 11d, table 2) is in a sample of pilotaxitic to hyalopilitic lava containing plagioclase, two pyroxenes, large hornblende grains with substantial opaque rims, and rare amounts of both rounded quartz grains and large anhedral olivine grains. The sample with lowest SiO_2 (11b, table 2) is a vesicular, porphyritic basaltic andesite with subhedral to euhedral phenocrysts of plagioclase, clino- and orthopyroxene, and hornblende in a fine-grained, holocrystalline groundmass. Hornblende also occurs in the groundmass and shows minor reaction rims of clinopyroxene but no opaque rims.

No regular variation of SiO_2 content with stratigraphic position is apparent in the pyroclastic-flow deposits (fig. 7B). The preserved volume of pyroclastic material in the deposits is estimated at 1.0 km^3, which classifies the deposits as intermediate in size (Aramaki and Yamasaki, 1963; Sheridan, 1979).

Figure 9. Prismatic fracturing of block in block-and-ash flow on east flank of Yantarni Volcano that occurred at elevated temperature of emplacement.

The porosity of juvenile clasts is low (see descriptions, fig. 8), implying a low degree of vesiculation and presumably a low explosivity of the eruptions that formed the pyroclastic flows.

Stereoscopic photopairs (fig. 10) show the surface morphology of the pyroclastic-flow deposits directly downslope from the cone. Although extensive erosion has occurred after deposition, sufficient unmodified surface remains to show the lobate distributary pattern of individual flows. Such a surface pattern is similar to that at Mount St. Helens (Rowley and others, 1981). In particular, we note the blocky, steep-fronted lobe that extends outward from a gully below the topographic high at the center of the figure (arrow); apparently here the pyroclastic flow channeled into the existing gully after crossing the low pass at the head of the gully. Inspection of the geologic map and photopairs suggests that the flows had little or no excess lateral momentum beyond that required to maintain mobility; the preserved deposits, for example, flowed into the opposing valleys but did not run up significant slopes.

Tephra deposits at two sites (stations 5 and 58, pl. 1) are provisionally correlated with the catastrophic Yantarni eruption: first, they are distinctly thicker or coarser than other tephra deposits at each site, and second, each deposit contains either diktytaxitic hornblende-bearing lava or altered porphyroaphanitic lava, both of which megascopically resemble clasts in the avalanche and pyroclastic-flow deposits. The four tephra samples (fig. 11) are better sorted than the pyroclastic-flow deposits (fig. 8), but only two tephra samples (5a and 5b) are sufficiently well sorted to plot wholly in the fall field and outside the pyroclastic-flow field of Walker (1971). Three of the four samples (5a, 5c, and 58a) are similar in their granulometric properties to the samples of pyroclastic-surge (directed blast) deposits at Mount St. Helens. The coarsest clasts in sample 58a are altered porphyroaphanitic lava, consistent with an origin in a carapace-destroying eruption. We cannot, however, unequivocally confirm a directed-blast origin because the most diagnostic evidence is the lateral distribution and internal structures of the deposit (Moore and Sisson, 1981; Hoblitt and others, 1981; Waitt, 1981). Owing to the high relief and severe climate, tephra deposits were not preserved for our ready identification at any other proximal localities.

To summarize, our data indicate that most of the pyroclastic flows were emplaced after a debris avalanche of cone material from the northeast sector of Yantarni cone. Blocks of cone material as much as tens of meters across are incorporated in the lowermost pyroclastic-flow deposits, suggesting that the initial pyroclastic flows were partly contemporaneous with avalanching. Debris avalanches are commonly but not necessarily accompanied by directed explosions (Siebert, 1984). We have found a possible but ambiguous candidate for a directed-blast deposit at one site 8 km southeast of the cone. Thus, we conclude that the debris avalanche was caused or at least closely followed by magmatic eruptive activity, but we cannot prove that the avalanche was accompanied by a directed blast.

Deposits of the debris avalanche and ensuing pyroclastic flows are certainly no older than Holocene by virtue of the absence of glacial erosion. The pyroclastic bed at site 58 that is provisionally correlated with the catastrophic eruption overlies silt with a radiocarbon age of about 2 ka (fig. 12). The radiocarbon age is a minimum, due to the presence of a trace amount of modern rootlets. Moreover, the pyroclastic bed lies atop silt (loess) that contains disseminated ash-sized clasts of white, gray, and honey-colored pumice and black obsidian. Such disseminated ash closely resembles, in its proportions of colors, proximal tephra deposits of the caldera-forming eruptions of Aniakchak Caldera collected at a site 30 km southwest of Yantarni Volcano (Riehle, unpublished data). The age of the Aniakchak eruption is between 3.3 and 3.7 ka (Miller and Smith, 1977), and if the correlation with site 58 is valid, then the coarse pyroclastic bed is no more than about 3,500 yr old. Thus, we provisionally consider the catastrophic eruption to be no more than 3,500 yr old and possibly as young as 2,000 yr.

Dome

The dome of Yantarni Volcano is about 1 km in exposed diameter and is centered in a semicircular amphitheater composed of the remains of the older cone (pl. 1; see frontispiece). The dome consists of pilotaxitic, hornblende-bearing andesite containing rare quartz phenocrysts(?) (samples 38 and 39, table 2). Hornblende grains range from euhedral ones having oxide rims to ones nearly completely replaced by assemblages of fine-grained plagioclase, pyroxene, and opaque grains. Whole-rock analyses indicate a high-silica andesitic composition (table 1).

We consider the dome to be the source of the pyroclastic-flow deposits, for two reasons. First, the dome (samples 38 and 39) petrographically resembles clasts in the matrix-depleted pyroclastic-flow deposits (samples 11b, 11c, 11d, and 14, table 2), and second, the surface of the pyroclastic plateau grades up to the apron of blocks surrounding the dome (see fig. 10 and pl. 1). Although we have inferred that a magmatic component of eruptive activity closely followed the debris avalanche, we cannot reconstruct the history of dome growth subsequent to the carapace-destroying eruption.

MAJOR-ELEMENT AND MINERAL COMPOSITIONS OF THE VOLCANIC ROCKS

Major-Oxide Variations

When whole-rock major-oxide contents are plotted on silica-variation diagrams (fig. 13), alumina, Fe_TO_3 (total iron), CaO, and MgO show some scatter, but all oxides vary linearly with SiO_2. The analytical variability of the data (that is, ± 2 sigma) is approximately the diameter of the plotted points (J.E. Taggart, Jr., oral commun., 1985). When analyses are plotted on various geochemical plots (fig. 14), the Yantarni analyses define a calc-alkaline trend. Following Peccarillo and Taylor (1976), we further classify the Yantarni samples as medium-K basaltic andesite, andesite, and dacite (fig. 14D).

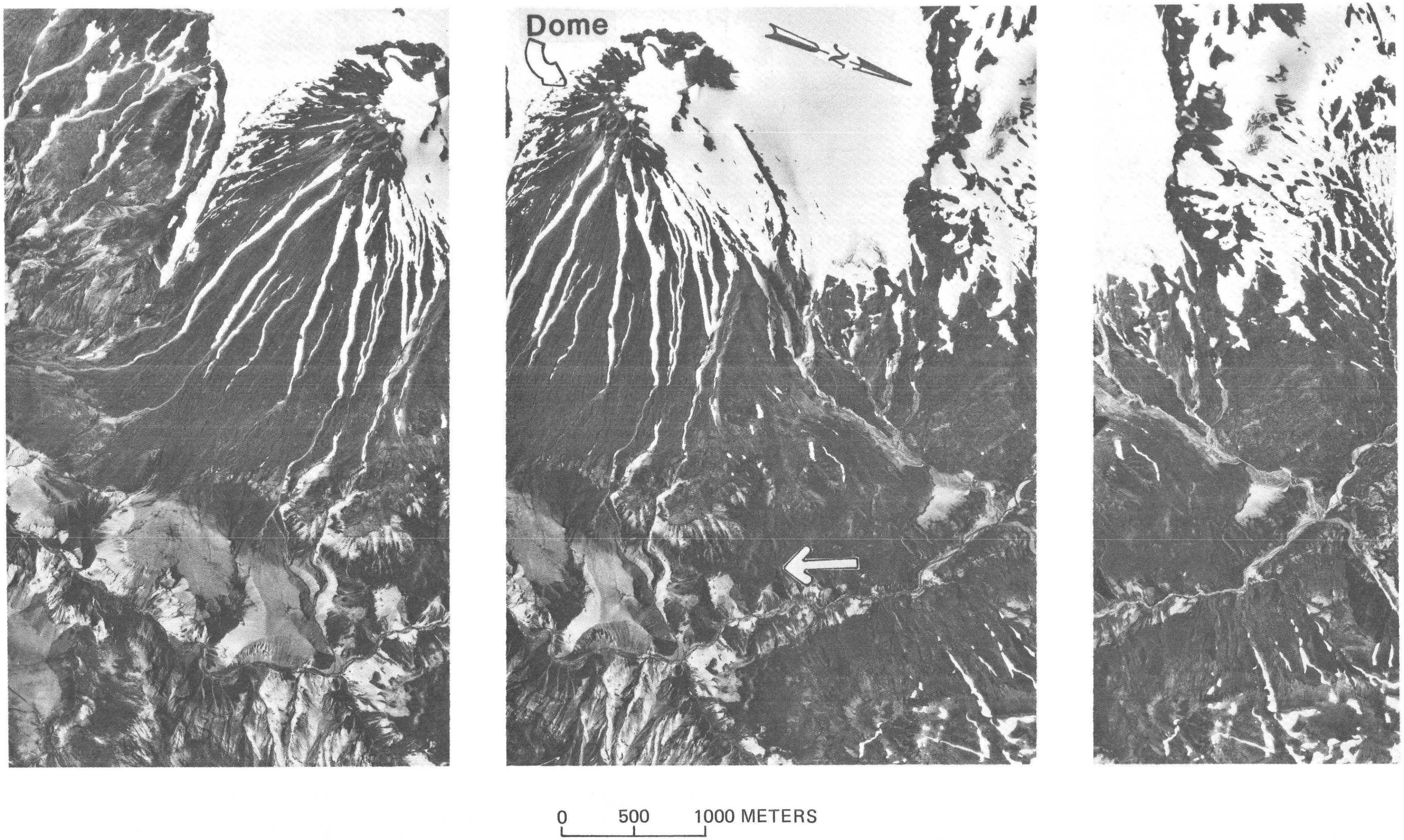

Figure 10. Stereopairs showing part of young pyroclastic-flow and debris-avalanche deposits, Yantarni Volcano. Arrow points to small, relatively unmodified lobe of pyroclastic-flow deposit.

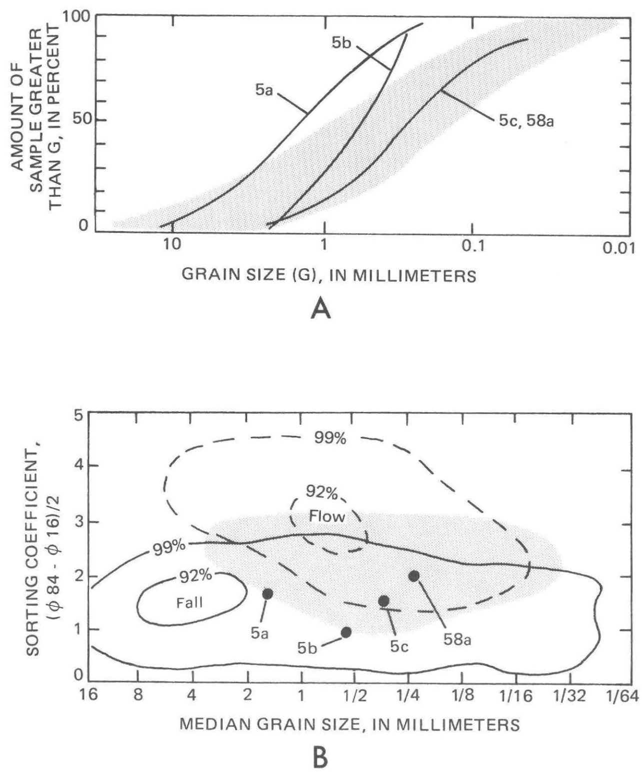

EXPLANATION

Megascopic petrographic descriptions of large juvenile clasts from sites 5 and 58 (pl. 1)--plag, plagioclase; hbl, hornblende; px, pyroxene

5a	Porphyry or vitrophyre, light gray, slightly vesicular to diktytaxitic; large phenocrysts of plag >hbl = px
5b, 5c	As above, plus a trace of red-brown scoria
58a	50 percent mineral grains including large unaltered hbl; 25 percent angular lapilli of altered porphyroaphanitic lava; 15 percent unaltered gray porphyry or vitrophyre, white to honey-colored pumice, and dark-gray scoria; remainder is a variety of sedimentary lithics and organic material

Figure 11. Granulometric data for proximal tephra deposits provisionally correlated with Yantarni Volcano. A, Grain-size distributions. Shaded area includes grain-size distributions of samples of directed-blast (surge) deposits, Mount St. Helens (Hoblitt and others, 1981). B, Median grain size versus sorting coefficient. Contours outline 92 and 99 percent of pyroclastic-flow and pyroclastic-fall samples of Walker (1971); shaded area is range reported by Hoblitt and others (1981) for directed-blast (surge) deposits, Mount St. Helens.

Uncommon lavas from elsewhere in the Aleutian arc, called "Aleutian magnesian andesites" by Kay (1978), are characterized by FeO*/MgO ratios of about 1.0 at 55-57 percent SiO_2. The most "primitive" Yantarni sample (11b, with a Thornton and Tuttle (1960) differentiation index (D.I.) of 38) has an FeO*/MgO ratio of 1.7. Thus, we conclude that no magnesian andesites, which are inferred to have erupted without interaction with island-arc crust (Kay, 1978), are among the Yantarni set.

We also compared selected aspects of major-element trends for Yantarni with those described by Kay and others (1982) for Aleutian volcanoes southwest of Yantarni. First, the average K_2O content of Yantarni samples at 57.5 percent SiO_2 is about 1.4 percent (fig. 13), less than the 2.0 percent for tholeiitic centers but identical to the 1.4 percent

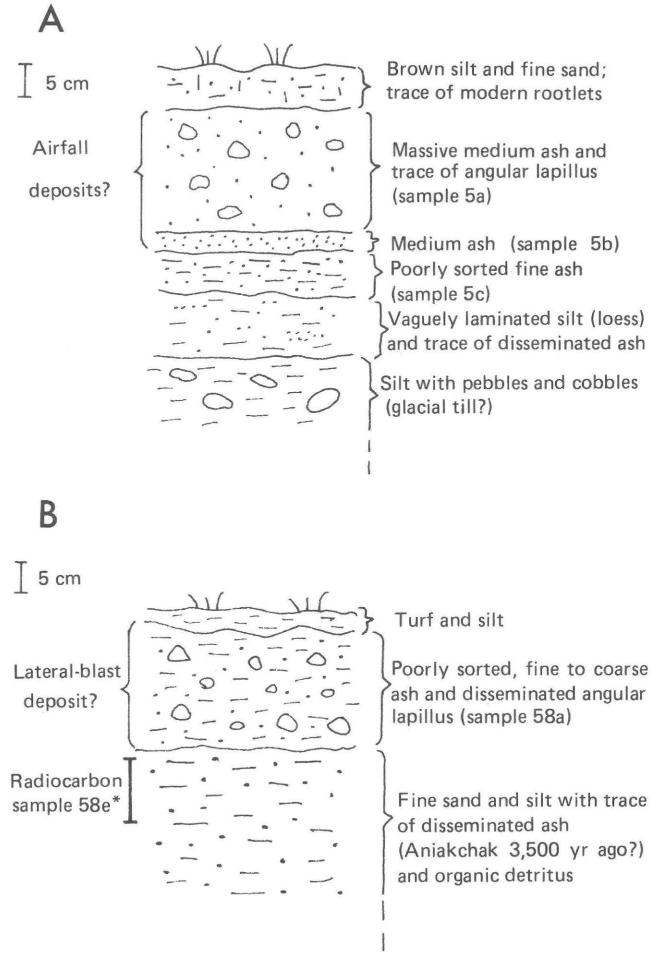

*2,010±80 years old (analysts: Teledyne Isotopes)

Figure 12. Measured sections of proximal tephra deposits at sites provisionally correlated with catastrophic eruption of Yantarni Volcano. For locations of sites see plate 1. Petrographic details and grain-size distributions of samples provided in figure 11. A, Site 5. B, Site 58.

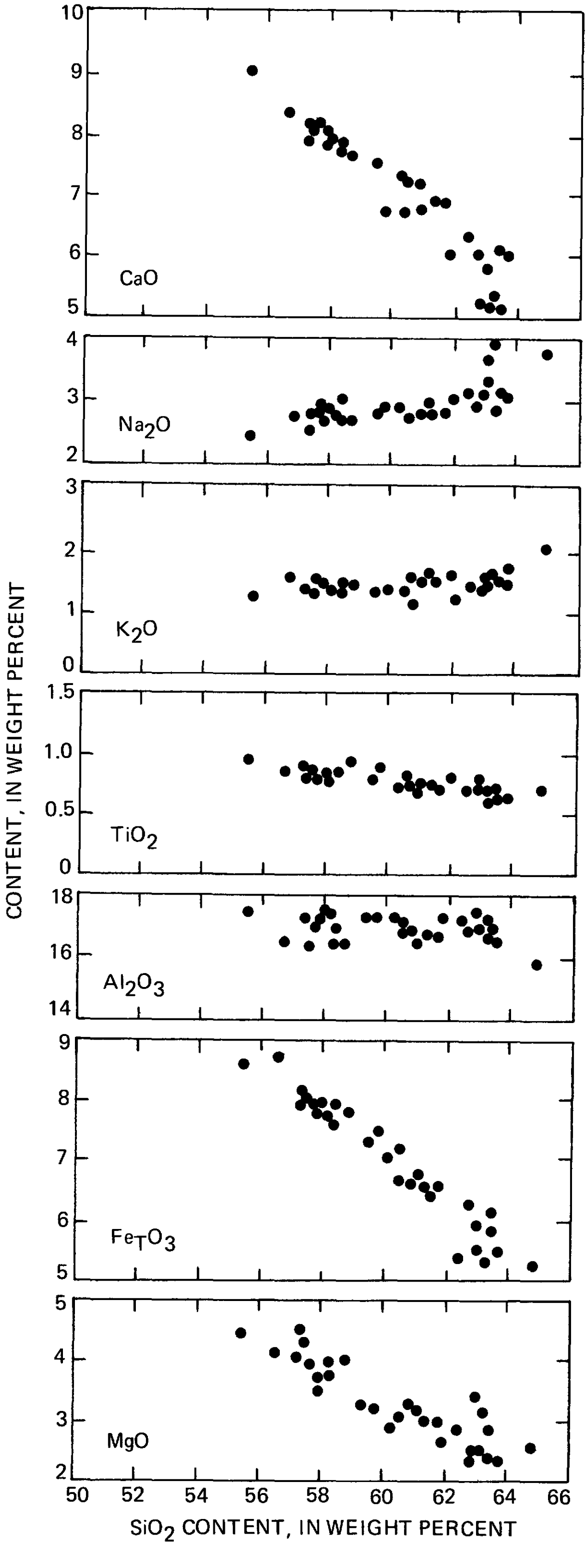

Figure 13. SiO_2-variation diagrams of Yantarni volcanic rocks. Plotted values are normalized to 100 percent on a volatile-free basis but including MnO and P_2O_5.

for calc-alkaline centers. Second, K_2O contents of the three samples of Tertiary hypabyssal rocks from the vicinity of Yantarni are similar to those of the younger Yantarni samples of similar SiO_2 contents (table 1), supporting the conclusion that no evidence exists for an evolutionary trend of K_2O with age in Aleutian samples. Third, Kay and others (1982) concluded that large, tholeiitic basaltic centers are more common at ends of arc segments whereas small, calc-alkaline andesitic centers are more common within arc segments. Application of this model suggests that Yantarni, a small calc-alkaline andesitic center, does not define the end of an arc segment such as one from Yantarni to Kialagvik (see fig. 2). Earthquake loci could provide a test of this hypothesis.

Mineral Compositions

Seven samples ranging from 56.9 to 63.1 percent SiO_2 were selected to survey the mineral compositions of Yantarni volcanic rocks for comparison with those of other medium-K calc-alkaline suites. Compositional data are also needed for crystal-fractionation modeling. Four of the seven samples (17, 19, 33, and 41) are from the cone-building deposits, two samples (11d and 12) are from the younger pyroclastic-flow deposits, and one sample (58) is from the dome.

Analyses were done on a nine-channel Applied Research Laboratories scanning electron microprobe Quantometer (ARL-SEMQ) using an on-line Bence-Albee matrix-correction program.[2] Backgrounds were calculated from on-peak counts on minerals of both higher and lower mean atomic number than the unknown but devoid of the element of interest. Standards used were a combination of natural and synthetic minerals. Analyses were done at 15 kV and 20 nA sample current measured on brass; count times were 10 seconds. Beam size was approximately 10 μm for feldspar analyses and the minimum possible (approximately 1 μm) for pyroxene, olivine, and amphibole analyses.

All seven samples contain both orthopyroxene and clinopyroxene, although samples 11d, 12, and 38 have less than 1 percent modal clinopyroxene. Compositions of Yantarni pyroxenes, plotted in figure 15 on a part of the pyroxene quadrilateral, fall within the compositional range expected for medium-K orogenic andesites (Gill, 1981, p. 174). Clinopyroxene compositions are remarkably constant across the 6 percent range of whole-rock SiO_2 values, falling in the fields of salite and high-Ca augite. Orthopyroxene grains define a slightly broader compositional range (En_{60-69}) in the hypersthene field. At least one sample (33) contains orthopyroxenes covering the entire range. As with the clinopyroxenes, orthopyroxene compositions show no correlation with whole-rock silica values.

[2]The use of trade names is for descriptive purposes only and does not constitute endorsement by the U.S. Geological Survey.

Representative pyroxene analyses (table 4) show that components other than Wo, En, and Fs are characteristically low. The typically low elemental concentrations of Al, Ti, and Na suggest crystallization at pressures no greater than 10,000 bars (Gill, 1981). Pyroxene grains in some of the samples show reverse zoning, with rims more magnesian than cores (see core-rim relations of two grains in sample 33, table 4). Changes in the physical and chemical conditions that may account for reverse zoning include magma mixing (Sakuyama, 1981), decompression (Ewart and others, 1975) and an increase in oxygen fugacity (Luhr and Carmichael, 1980).

Olivine is found in both the sample of highest and the sample of lowest SiO_2 content of the seven examined in detail (analyses are projected onto the pyroxene quadrilateral of fig. 15). The compositional range of olivine cores (table 5) from Yantarni samples is notably small (Fo_{80-81}), and the cores are more magnesian than expected for equilibrium at surface conditions based on the coexisting pyroxenes or whole-rock chemistry. The olivine analyzed in sample 11 is clearly out of equilibrium with the bulk-rock composition (assuming a distribution coefficient (Roeder and Emslie, 1970) of K_D = 0.30) and with coexisting orthopyroxene. The olivine grains in sample 11 must have crystallized in a more "primitive" liquid and presumably were included in a more differentiated magma by mechanical means.

Plagioclase is the dominant phenocryst phase in all samples and is complexly zoned; thus, the few analyses performed in this study probably do not adequately define the compositional variation that may be present. They do, however, give an approximation of the plagioclase compositions (table 6, fig. 16). Analyses range from An_{87} to An_{49} within the suite of samples studied. Within-sample variation, greatest in sample 17, is as large as 25 mole percent

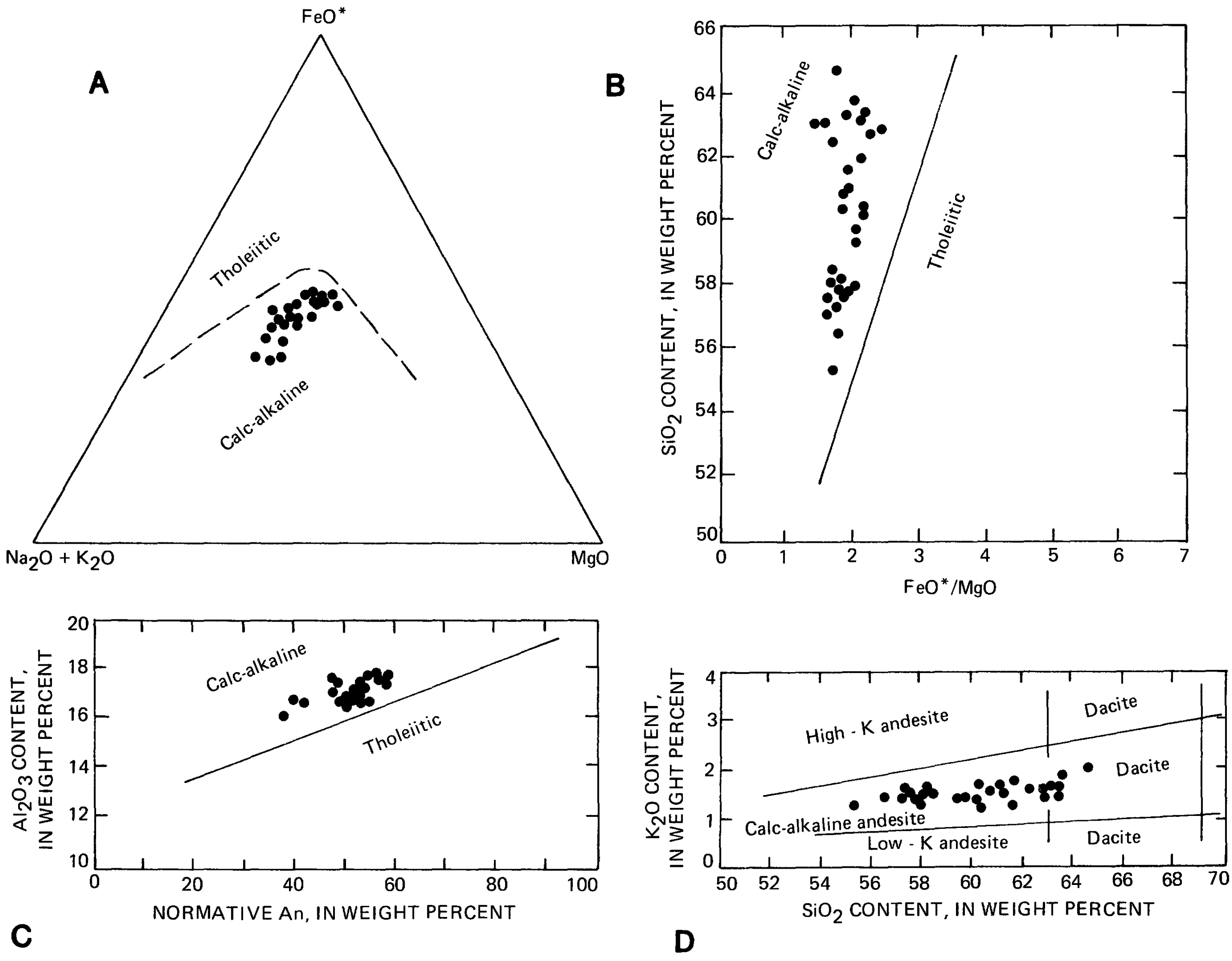

Figure 14. Classification plots of all Yantarni samples. A, FMA plot. Field boundary from Irvine and Baragar (1971). FeO* = FeO + $0.9Fe_2O_3$. B, FeO*/MgO versus SiO_2. Field boundary from Miyashiro (1974). C, Al_2O_3 versus normative An. Field boundary from Irvine and Baragar (1971). D, K_2O–SiO_2 classification (Peccerillo and Taylor, 1976).

An. Cores in most samples vary less than 10 mole percent An and fall in the range An_{50-60}.

In sample 11d, six cores fall between An_{52} and An_{58} and two others contain An_{68} and An_{73}, suggesting a bimodal distribution. Despite core heterogeneity, the four rims that were analyzed have An contents less than 51 mole percent. More data are necessary to determine whether this sample does have a bimodal distribution of plagioclase compositions (see for comparison Sakuyama (1981), who analyzed 100 plagioclase cores per sample).

Hornblende is present in small amounts in five of the seven samples analyzed (four representative analyses are presented in table 7). Because microprobe analyses determine total iron, and because the proportions of ferric and ferrous iron affect the mineral norm, it is necessary to estimate the ferric iron content on stoichiometric considerations. Therefore, the weight percent oxide values were recast using RECAMP (Spear and Kimball, 1984) to arrive at stoichiometric limits for Fe^{3+} content, shown in table 7.

Yantarni amphiboles are calcic, having Ca in excess of 1.7 per 32 oxygen. Silicon values are at the high end of the normal range for orogenic andesites, 6.8 to 7.1 per 32 oxygen. Such Si values are typical of continental-arc, as opposed to island-arc, volcanoes (Gill, 1981).

The first major phase to crystallize in all Yantarni samples is probably plagioclase, as inferred from its occurrence as small anhedral inclusions in all

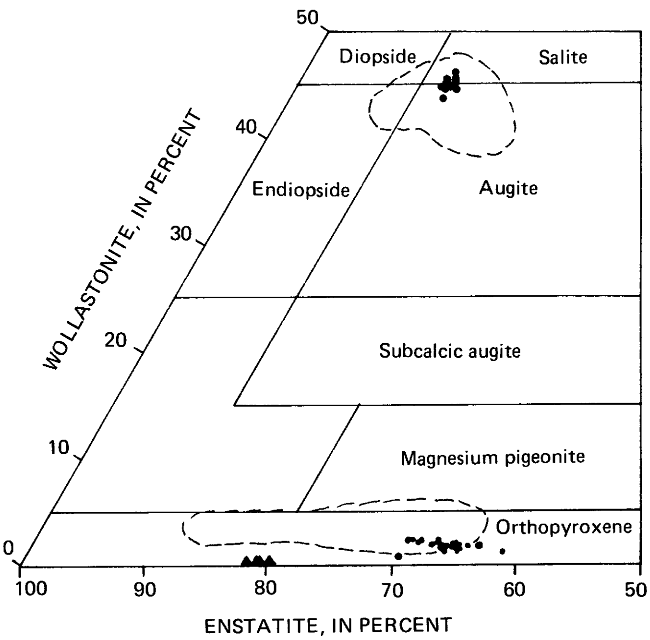

Figure 15. Pyroxene quadrilateral showing compositions of cores of clinopyroxene and orthopyroxene grains from lavas of Yantarni Volcano, relative to that of other medium-K calc-alkaline andesites (dashed lines; Gill, 1981). Olivine analyses (triangles) are projected onto baseline.

Table 4. Analyses of representative pyroxene phenocrysts from Yantarni Volcano

[Iron partitioning and structural distribution by the method of Papike and others (1974). exoct, excess of cations beyond those necessary to fill the octahedral site; quad, percentage of total cations accounted for in the pyroxene "quadrilateral" (Wo-En-Fs); other, percentage of cations other than those of the pyroxene quadrilateral]

	Sample No.					
	33		33		17	17
	(core)	(rim)	(core)	(rim)	(core)	(core)
SiO_2	52.5	52.9	53.4	54.1	52.2	53.0
Al_2O_3	1.12	1.11	0.85	0.47	1.04	0.71
TiO_2	0.20	0.23	.10	.23	0.28	.17
FeO	9.29	8.79	20.0	19.0	9.2	20.1
MnO	.49	.36	1.68	.98	.45	.77
MgO	14.4	15.0	24.1	25.1	14.9	24.0
Cr_2O_3	.01	.00	.00	.00	.00	.00
CaO	21.6	21.6	.47	1.04	21.5	1.2
Na_2O	.29	.29	.01	.03	.30	.03
Total	99.9	100.3	100.6	101.0	99.9	100.0
	Cations calculated on the basis of 6 oxygens					
Si	1.957	1.957	1.960	1.970	1.946	1.958
Al^{IV}	0.043	0.043	0.037	0.020	0.046	0.031
Al^{VI}	.006	.006	.000	.000	.000	.000
Fe^{2+}	.242	.227	.582	.569	.235	.598
Fe^{3+}	.047	.045	.032	.010	.052	.024
Mg	.800	.827	1.318	1.362	.828	1.322
Mn	.015	.011	.052	.030	.014	.024
Ti	.006	.006	.003	.006	.008	.005
Cr	.000	.000	.000	.000	.000	.000
exoct	.116	.123	.987	.977	.137	.972
a	.863	.856	.018	.041	.859	.048
Na	.021	.021	.001	.002	.022	.002
quad	94.12	94.3	96.32	97.98	94.05	96.91
other	5.88	5.7	3.68	2.02	5.95	3.19
wo	45.3	44.8	1.0	2.1	44.7	2.4
en	42.0	43.3	68.7	69.1	43.1	67.2
fs	12.7	11.9	30.3	28.9	12.2	30.4

Table 5. Analyses of representative olivine phenocrysts from Yantarni Volcano

	Sample No.		
	19	12	11
	(core)	(core)	(core)
SiO_2	39.2	39.2	38.9
FeO	18.1	18.7	18.6
MgO	42.8	42.2	42.2
CaO	0.14	0.14	0.14
MnO	.29	.28	.27
NiO	.07	.05	.06
Total	100.6	100.6	100.3
Cations calculated on the basis of 4 oxygens			
Si	0.994	0.996	0.993
Fe	.384	.398	.397
Mg	1.617	1.599	1.606
Ca	.004	.004	.004
Mn	.006	.006	.006
Ni	.001	.001	.001
fo	80.4	79.7	79.7
mg	80.8	80.1	80.2

other silicate phenocrysts except olivine. Inclusions occur in plagioclase in all samples and are small, irregular or rounded blebs of subopaque material that is presumably devitrified glass. Most samples show a range from inclusion-free plagioclase, to grains with minor concentric zones of inclusions, to grains with interiors full of inclusions (fig. 17).

The high abundance of phenocrysts in all samples except 11b makes it difficult to generalize further about the relative order of crystallization. Sample 11b has the lowest SiO_2 content among the sample set (55.5 percent) and contains only 12 percent by volume phenocrysts; oddly, it has no olivine. Hornblende phenocrysts in 11b are more abundant and are two to three times greater in size than clinopyroxene, which suggests that hornblende preceded clinopyroxene in this sample. Reaction rims of pyroxene and plagioclase on some hornblende grains in all hornblende-bearing samples indicate that the magmas were out of equilibrium with at least a particular composition of hornblende prior to eruption. Hornblende, however, occurs also as microphenocrysts in sample 11b despite the occurrence of minor reaction rims on phenocrysts (fig. 18); thus, some composition of hornblende apparently remained as a liquidus phase in this sample until eruption.

Orthopyroxene commonly occurs as both euhedral phenocrysts and micro-phenocrysts. No evidence bearing on the age of orthopyroxene relative to hornblende has been obtained from any sample. Rims of clinopyroxene on orthopyroxene occur rarely in most samples, but such a texture does not prove that orthopyroxene preceded clinopyroxene during crystallization. Quartz occurs as mosaics of anhedral grains, probably xenoliths, in two of three samples of the Tertiary hypabyssal rocks but has not been observed in the older lavas. Quartz occurs as rare rounded single grains in two samples of the cone-building unit and more commonly in samples of the younger pyroclastic flows and dome (see table 2). Olivine occurs only rarely, as irregular anhedral phenocrysts and microphenocrysts with no inclusions, in the cone-building lavas and in the younger pyroclastic flows and dome. In sample 11d, which also contains quartz phenocrysts, the olivine microphenocrysts have incipient reaction rims of

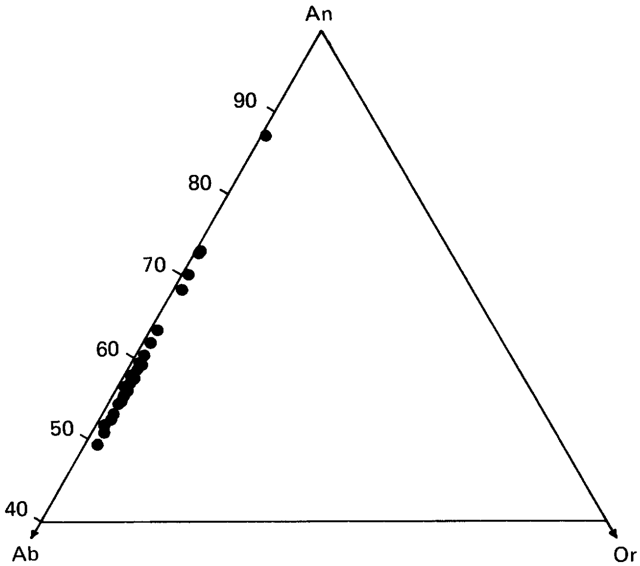

Figure 16. Part of albite(Ab)-anorthite(An)-orthoclase(Or) feldspar diagram showing compositions of cores of plagioclase grains from Yantarni volcanic rocks.

Table 6. Analyses of representative plagioclase phenocrysts from Yantarni Volcano

	Sample No.						
	11 (core)	11 (core)	17 (core)	19 (core)	33 (core)	33 (core)	38 (core)
SiO_2	54.0	50.1	46.1	52.8	55.3	53.7	55.6
Al_2O_3	29.0	32.2	33.9	29.7	28.2	29.1	27.6
FeO	0.27	0.29	0.45	0.42	0.23	0.33	0.26
CaO	11.6	15.0	17.9	12.8	10.8	12.1	10.1
Na_2O	4.90	3.04	1.41	4.26	5.46	4.62	5.61
K_2O	.20	.08	.02	.15	.16	.18	.27
Total	100.0	100.7	99.8	100.1	100.2	100.0	99.4
	Cations calculated on the basis of 32 oxygens						
Si	9.774	9.087	8.524	9.578	9.963	9.726	10.072
Al	6.186	6.883	7.387	6.350	5.988	6.212	5.893
Fe	0.041	0.044	0.070	0.064	0.035	0.050	0.039
Ca	2.249	2.915	3.546	2.488	2.085	2.348	1.960
Na	1.720	1.069	.505	1.498	1.907	1.622	1.970
K	.046	.019	.005	.035	.037	.042	.062
an	56.0	72.8	87.4	61.9	51.7	58.5	49.1
ab	42.8	26.7	12.5	37.3	47.3	40.4	49.3
or	1.2	.5	.1	.9	.9	1.0	1.6

Table 7. Analyses of representative amphibole phenocrysts from Yantarni Volcano

	Sample No.							
	38 (core)		41 (core)		33 (core)		12 (core)	
SiO_2	48.6		47.5		48.6		47.6	
Al_2O_3	6.8		7.9		7.2		7.8	
FeO	13.1		12.8		13.0		13.2	
MgO	15.3		15.3		15.3		14.7	
MnO	0.39		0.27		0.62		0.37	
TiO_2	1.26		1.64		1.02		1.59	
CaO	11.3		11.5		11.4		11.2	
Na_2O	1.20		1.99		1.16		1.27	
K_2O	.34		.37		.38		.39	
Total	98.2		99.3		98.7		98.1	
	Magnesian hornblende		Edenite	Magnesian hornblende	Magnesian hornblende		Magnesian hornblende	
	Sum CA=15	Si+Al=8	All Fe^{2+}	Sum FM+13	Sum CA=15	Sum FM+13	Sum CA=15	Sum FM=13
Si	7.001	6.867	6.843	6.728	6.991	6.863	6.915	6.781
Al^{IV}	0.999	1.133	1.157	1.272	1.009	1.137	1.085	1.219
Al^{VI}	.156	0.000	0.184	0.047	0.213	0.062	0.251	0.091
Ti	.137	.134	.178	.175	.110	.108	.174	.170
Fe^{3+}	.173	1.047	.000	.772	.182	1.022	.057	.946
Mg	3.285	3.222	3.285	3.230	3.280	3.220	3.183	3.121
Fe^{2+}	1.405	.501	1.542	.745	1.382	.514	1.547	.627
Mn	.109	.107	.033	.032	.076	.074	.046	.045
SumFM	13.264	13.010	13.222	13.000	13.243	13.000	13.257	13.000
Ca	1.736	1.703	1.775	1.745	1.757	1.725	1.743	1.710
NaM_4	.000	.286	.003	.255	.000	.275	.000	.290
Na_{tot}	.335	.329	.556	.547	.324	.318	.358	.351
Na_A	.335	.043	.553	.292	.324	.043	.358	.060
K	.062	.061	.068	.067	.070	.068	.072	.071
sum A	.398	.104	.621	.359	.393	.111	.430	.131
Fe^{2+}/Fe^{2+}+Mg	.300	.134	.319	.187	.296	.138	.327	.167

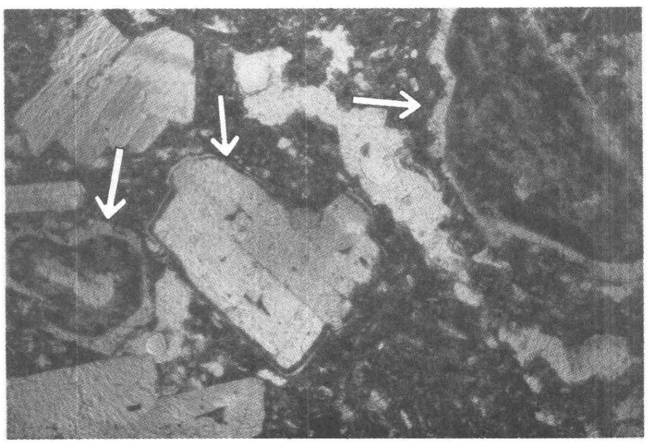

Figure 17. Photomicrograph of dacite block from Yantarni pyroclastic-flow deposit showing typical inclusions, probably devitrified glass, in plagioclase. Grain on left (arrow) has extensive inclusions within a narrow inclusion-free rim, that on right (arrow) has an interior zone of inclusions, and grain at center has only a narrow band of inclusions near its margins. Width of view, 3.5 mm. Uncrossed polars; sample 14.

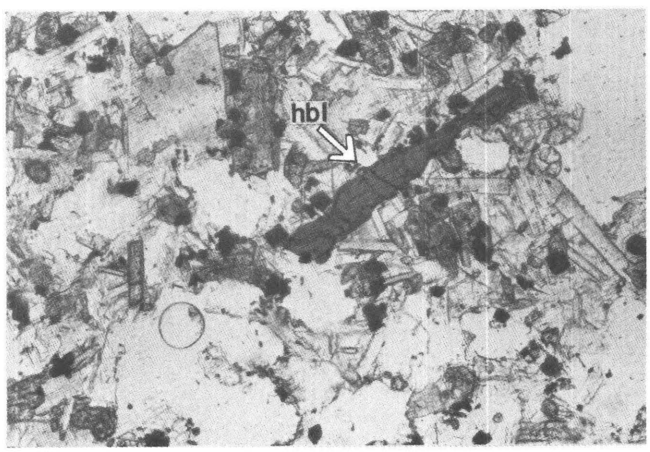

Figure 18. Photomicrograph of Yantarni basaltic andesite showing an unaltered hornblende microphenocryst (hbl) in fine-grained groundmass. Width of view, 1.5 mm. Uncrossed polars; sample 11b.

pyroxene (fig. 19), supporting the previous conclusion that the olivine in 11d is not in equilibrium with its whole-rock composition. Quartz grains in some samples are surrounded by rims of fine-grained clinopyroxene (fig. 20), suggesting that clinopyroxene stability was favored by higher silica activity.

The lithic inclusions in the Yantarni lavas (table 2) fall into two types: (1) fine-grained mosaics in which pyroxene exceeds plagioclase and opaque minerals (fig. 21A), and (2) fine- to medium-grained, diabasic clasts (plagioclase > subophitic pyroxene > opaque) and pyroxenitic clasts (fig. 21B). The first type greatly resembles reaction rims on hornblende grains and probably is completely reacted hornblende. The second type is probably cognate (accessory) inclusions.

Obvious correlations of modal occurrence with SiO_2 content (fig. 22) are few: quartz occurs more commonly, and olivine is less abundant, in samples having more than 60 percent SiO_2. Hornblende is more abundant in samples having more than 60 percent SiO_2 but occurs in a few samples that incorporate the entire range of SiO_2 contents; we note that hornblende in the groundmass of an andesitic arc magma (11b) has been thought to be uncommon (Gill, 1981, p. 179). Orthopyroxene and clinopyroxene appear to decrease from 57 percent to 63 percent SiO_2. Neither plagioclase abundance nor opaque-minerals abundance show any variation with SiO_2 content. The absence of olivine from sample 11b (55.5 percent SiO_2) could be due to reaction with orthopyroxene during cooling, as occurred during experimental crystallization of an andesite containing 60 percent SiO_2 (Eggler, 1972). Such a hypothesis, however, does not explain the occurrence of olivine in Yantarni samples of higher SiO_2 and phenocryst contents. In particular, the occurrence of euhedral microphenocrysts of olivine in sample 11d (63.7 percent SiO_2) implies that olivine was a liquidus phase in this sample until shortly before eruption, despite the high silica content.

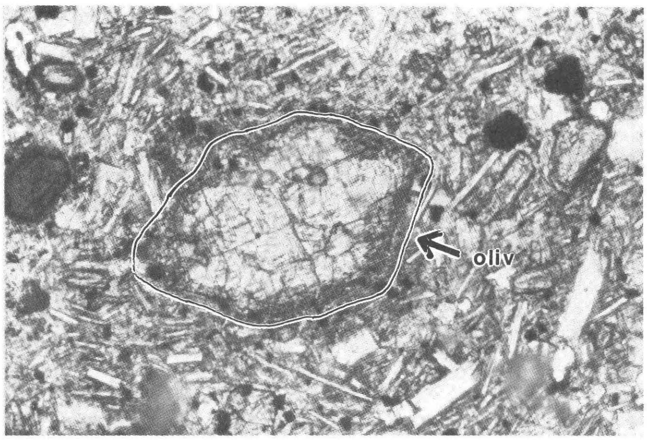

Figure 19. Photomicrograph of Yantarni low-silica dacite showing olivine microphenocryst (oliv) with a narrow reaction rim of pyroxene. Despite high silica content of rock (63 percent), olivine apparently crystallized shortly before eruption. Width of view, 1.5 mm. Uncrossed polars; sample 11d.

Origin of the Chemical Trends

The origin of the major-element variation at Yantarni Volcano is not amenable to a unique solution with our available data. We have not, therefore, carried out quantitative calculations of the composition of various mineral-magma pairs. We can, however, limit the potential role of closed-system fractionation in generating the Yantarni chemical trends by the following reasoning. A wide range of bulk phenocryst compositions can be postulated by combining differing amounts of plagioclase, orthopyroxene, olivine, and hornblende (the earliest phases to crystallize). The greatest K_2O content of such postulated mineral assemblages is 0.4 percent in pure Yantarni hornblende (table 3). By inspection of the K_2O variation diagram (fig. 23), it is apparent that the K_2O trend of Yantarni cannot be produced from an assumed parent of 11b (having the lowest D.I. and SiO_2 content among the analyzed samples), even by removal of pure hornblende. In fact, crystallization of hornblende was probably preceded by plagioclase in 11b, and no reasonable combination of preserved

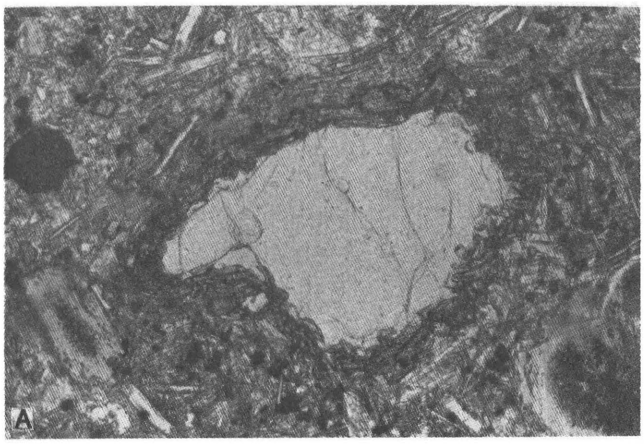

Figure 20. Photomicrographs of high-silica andesite composing Yantarni dome, showing quartz grain surrounded by a narrow reaction rim of clinopyroxene. Width of views, 1.5 mm; sample 39. A, Uncrossed polars. B, Crossed polars.

phenocrysts in 11b can produce the Yantarni K_2O-SiO_2 trend. Thus, if the variation trend is the result mainly of closed-system fractionation by preserved phenocrysts of a basic parent, we have not sampled such a parent. Moreover, the slope of several of the variation trends is such that no analyzed samples are likely to be related to one another by simple fractionation involving preserved phenocrysts. This assertion follows from the geometric constraint that both the parent magma and the bulk composition of the fractionated (removed) solids must be colinear with each variation trend.

As previously discussed, analyzed Yantarni hornblendes are relatively high in SiO_2, similar to other continental-arc hornblendes. Hornblende grains in xenolithic inclusions in calc-alkaline island-arc andesite from Adak Island, however, have much lower SiO_2 contents at similar K_2O contents (Conrad and Kay, 1984) and the oxide contents of these hornblendes are in fact approximately colinear with most Yantarni variation trends (fig. 23). We have no independent data with which to evaluate the potential role of such island-arc-type hornblendes in the genesis of Yantarni magmas, but it is possible to postulate ad hoc mineral compositions that are colinear with Yantarni trends. Yet another alternative to generate the Yantarni trends is by removal of chemically different batches of magma from a single parent (open-system fractionation). As an example, we note that a parent magma with K_2O-SiO_2 in the shaded region on figure 23 could yield low-silica Yantarni samples by removal of Yantarni hornblende. High-silica Yantarni samples could be generated by removal of some unspecified mineral assemblage, lower in both K_2O and SiO_2 than Yantarni hornblende.

We conclude that Yantarni variation trends cannot be generated by simple closed-system fractionation of one sample from another by the observed phenocryst phases. The samples could be

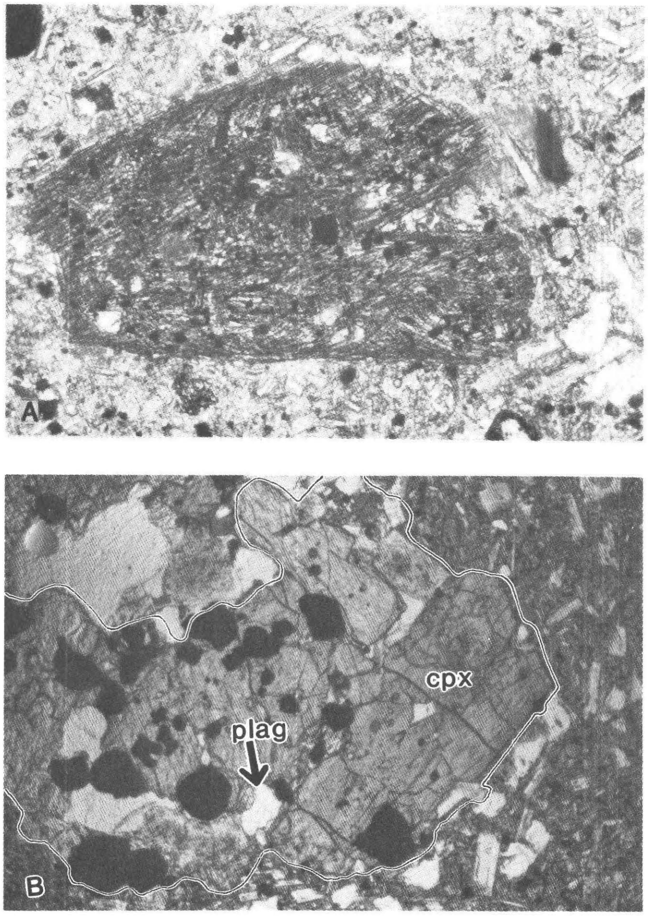

Figure 21. Photomicrographs illustrating two types of lithic inclusions in Yantarni lavas. Crossed polars. A, Fine-grained plagioclase-pyroxene pseudomorph after hornblende. Width of view, 1.5 mm; sample 39. B, Medium-grained pyroxenitic inclusion, probably a cognate xenolith. plag, plagioclase; cpx, clinopyroxene. Width of view, 3.5 mm; sample 16.

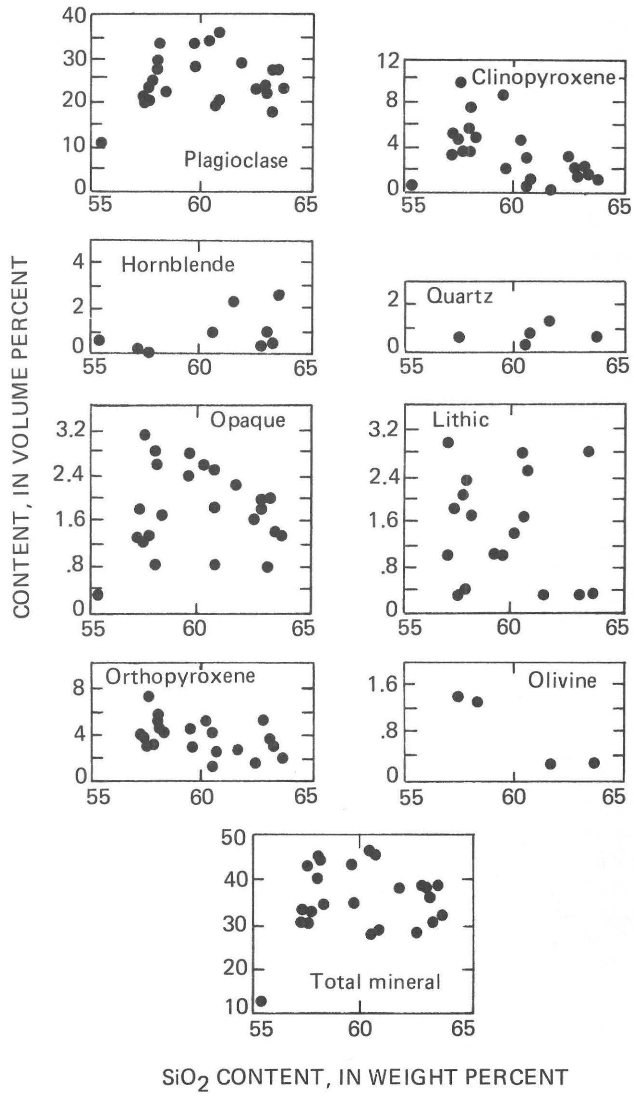

Figure 22. Phenocryst modes, lithic abundances, and total phenocryst contents plotted against whole-rock SiO_2 content (volatile-free) for Yantarni lavas. No plotted quantity shows any consistent correlation with SiO_2.

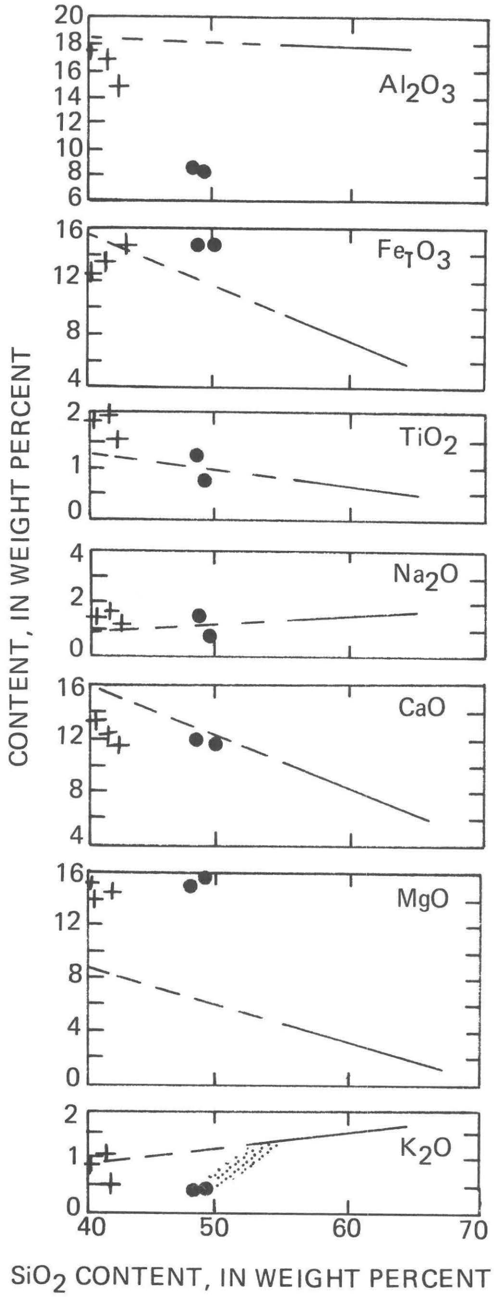

Figure 23. SiO_2-variation diagrams of Yantarni whole-rock analyses (solid lines are least-squares regressions; dashed lines are extrapolations), Yantarni hornblende analyses (solid dots), and analyses of hornblendes in xenoliths from calc-alkaline andesites, Adak Island, Aleutian volcanic arc (crosses) (Conrad and Kay, 1984). Maximum K_2O content of all possible Yantarni phenocryst assemblages is 0.40 percent in pure hornblende, thus, K_2O-SiO_2 diagram indicates that Yantarni magmas could not have been generated by closed-system fractionation of a single parent by analyzed Yantarni phenocrysts. Hypothetical parent magmas plotting in shaded region of K_2O-SiO_2 diagram, however, could yield low-silica Yantarni samples by removal of Yantarni hornblende; therefore, SiO_2-variation diagrams do not preclude generation of Yantarni magmas by open-system fractionation.

generated from a single unsampled parent by removal of batches of magma that have undergone differing degrees of fractionation (open-system fractionation), each batch resulting in a different sampled composition. We cannot model such open-system fractionation because without knowing the composition of the parent magma the model is wholly unconstrained. Alternatively, the variation trends can also be produced by invoking ad hoc mineral compositions.

Conversely, another process to generate the observed variation diagrams is mixing of discrete magmas or magma and solid rock such as crustal blocks. A necessary but not sufficient test for mixing of two end members is linearity of variation plots (Eichelberger, 1974). To test our data for linearity we have used a regression program to fit the data by a least-squares technique by lines and by simple quadratic curves. The goodness of fit for both lines and curves is given by the residuals in table 8. We conclude that the variation of all major elements is fitted nearly as well by a line as by a quadratic curve and that the chemical data permit mixing as a major cause of variation.

In support of a mixing model, we note the following aspects of the chemical and mineralogic data:

1. The occurrence of a disequilibrium assemblage of quartz and forsteritic olivine in a single sample (11d, table 2) of the young dacitic pyroclastic-flow deposits.

2. The occurrence of the lowest and highest SiO_2 contents among the samples as lava flows stratigraphically high in the cone-building deposits (samples 19 and 41) and in the succeeding pyroclastic-flow deposits (samples 11b and 11d): magmas differing by 8 percent in SiO_2 content existed nearly simultaneously in the conduit(s) or reservoirs.

3. Reacted hornblende, reverse zoning in mafic phenocrysts, and rounded olivine and quartz grains are common in Yantarni samples; such textures can result from changes of parameters such as pressure but can also result from disequilibrium as a consequence of mixing.

4. Neither phenocryst modes nor total phenocryst contents show systematic variation with SiO_2, implying that the composition of Yantarni magmas was not governed mainly by crystal-liquid equilibrium.

5. Quartz xenoliths occur in the Tertiary hypabyssal rocks; although such foreign material is absent from later extrusive rocks, its presence in the early rocks indicates that assimilation has clearly occurred.

The absence of banded pumice at Yantarni Volcano could weigh against the mixing hypothesis; however, we have found no more than a few percent glass in any sample, including those of the pyroclastic flows, and we conclude that any color banding would have been obscured by crystallization.

Table 8. Residual sums of squares for each of seven major oxides regressed against SiO_2

[A quadratic expression fits the variation plots only slightly better than a linear expression. Regressions performed by Merribeth Bruntz, U.S. Geological Survey]

	Al_2O_3	Fe_TO_3	MgO	CaO	Na_2O	K_2O	TiO_2
Linear fit	3.77	1.84	1.78	2.84	1.02	0.45	0.08
Quadratic fit	3.76	1.77	1.68	2.75	1.00	.45	.08

To summarize, we cannot prove that major-element variation in Yantarni rocks is a result of a single process. However, the available data (1) preclude an origin by progressive fractionation of one sample from another involving observed phenocryst phases, (2) support, but do not prove, the viability of mixing as a mechanism to generate the observed compositions, and (3) neither support nor preclude open-system fractionation or fractionation involving mineral compositions other than those analyzed.

GEOLOGIC HISTORY OF YANTARNI VOLCANO

Volcanism in the vicinity of Yantarni Volcano has occurred sporadically since late Tertiary time. Intrusion of shallow sills, dikes, and small stocks occurred in early Miocene and early Quaternary time (F.H. Wilson, oral commun., 1985) and presumably such intrusive activity was accompanied by extrusion of lava, now eroded. Limited chemical data indicate a low-silica dacitic composition of such early hypabyssal rocks in the close vicinity of Yantarni Volcano (table 1; F.H. Wilson, oral commun., 1985). A single Miocene radiometric age is the basis for assigning the older part of the hypabyssal activity to the predecessor of the modern Aleutian arc (Wilson, 1985).

The oldest preserved extrusive deposits are andesitic lava flows of middle Pleistocene age. The source vents of such flows are poorly known; some may have erupted from vents at the site of present Yantarni Volcano, but others erupted from vents mapped beyond the margins of the cone.

The onset of central-vent volcanism is indicated by basal pyroclastic-flow deposits in the cone of Yantarni Volcano. A single radiometric age from the basal deposits (0.46 Ma) overlaps within uncertainty with two age determinations of the older lava flows (0.47 Ma and 0.62 Ma); thus, the two phases of volcanism either overlapped or followed in close succession. A single age from deposits stratigraphically high in the cone-building unit (0.41 Ma) overlaps within uncertainty with the age of the basal cone deposits. The two radiometric ages are consistent with the inference drawn from the degree of glacial erosion of the cone that cone construction was largely completed before late Pleistocene glaciation. Major-element compositions of the basal cone deposits are similar to those of the older lava flows.

The latest phase of significant eruptive activity apparently began with failure and mass movement of the northeast sector of the cone in a debris avalanche. The avalanche was closely followed by the first of several pyroclastic flows, which probably originated both by nonexplosive dome collapse and by low-explosivity eruptions accompanying dome growth. The debris avalanche, which may have been accompanied by a directed blast, is no older than Holocene and may have occurred within the past 3,500 yr.

Magmas of the cone-building stage reach a maximum of about 64 percent SiO_2, a higher SiO_2 content than has been found in both the older flows and the basal cone deposits. Such high-SiO_2 lavas also occur in the early hypabyssal rocks, however, thus no evidence exists for a consistent long-term trend in the SiO_2 content of magmas emplaced at or near Yantarni Volcano. One of the lowest SiO_2 contents of the sample set occurs late in the cone-building phase, and the full range of SiO_2 contents of the sample set is present in pyroclastic deposits formed during the catastrophic eruption in late Holocene time. Indeed, if there is a temporal trend in composition of lavas at Yantarni Volcano, it is toward increasing heterogeneity.

Estimated volumes of Quaternary eruptive products are subject to large uncertainty owing to poorly known thicknesses. Our estimates (0.6 km^3 of preserved middle Quaternary lava flows, as much as 6.6 km^3 of cone material before erosion, and 1.0 km^3 of pyroclastic-flow material) yield an aggregate volume of 8.2 km^3 and indicate that Yantarni Volcano is one of the smaller Aleutian volcanoes (see summary of volume estimates by Marsh, 1982, fig. 4).

CONCLUSIONS

1. Yantarni Volcano is a small andesitic stratovolcano of the eastern Aleutian volcanic arc; the magmas are calc-alkaline and support the classification of Yantarni as an intra-segment volcanic center. No samples of primitive "magnesian andesite" reported by Kay and others (1978) from elsewhere in the Aleutian arc have been found at Yantarni Volcano.

2. Magmatism at the site began with shallow intrusions of dacitic magma as early as about 20 Ma; such activity has been assigned to the predecessor of the modern Aleutian arc (Wilson, 1985). The early activity includes magmas with SiO_2 contents as high as the most siliceous of the recent eruptive products.

3. Magmatism clearly assignable to the modern Aleutian arc began at the site at perhaps 4 Ma, and at about 0.60 Ma the oldest extrusive rocks were erupted from a number of local vents.

4. At about 0.46 Ma, volcanism entered a central-vent phase of cone-building, identifiable by lithic pyroclastic-flow deposits suggestive of dome collapse. Such pyroclastic deposits are andesitic, similar in major-element composition to the

slightly older lava flows. This phase of cone-building apparently ended before the last extensive glaciation in late Pleistocene time.

5. The latest significant activity began with failure of the northeast sector of the cone, leading to a debris avalanche possibly accompanied by a directed blast. The avalanche was closely followed by the first of a succession of pyroclastic flows generated by growth of a dome. Such a catastrophic eruption probably occurred no more than about 3,500 years ago, and we consider the volcano to have the potential for a return to eruptive activity of similar style and magnitude.

6. Low contents of Al, Ti, and Na in pyroxene phenocrysts indicate crystallization at pressures below 10,000 bars. The occurrence of lavas with both the highest and lowest SiO_2 contents of the entire sample set in the youngest deposits indicates the coexistence of two or more magmas. Olivine microphenocrysts having incipient reaction rims are associated with rounded quartz phenocrysts in the young pyroclastic-flow deposits, strongly implying mechanical incorporation shortly before eruption.

7. Relations among whole-rock compositions and coexisting phenocryst compositions indicate that the range of chemical variability in Yantarni magmas is not likely the result of closed-system fractionation of one sample from another. Conversely, mixing of two end-members is permitted by the linearity of the SiO_2-variation diagrams and is circumstantially supported by reverse zoning of mafic phenocrysts and by disequilibrium mineral assemblages.

8. The preceding conclusions suggest that no large, homogeneous magma chamber exists at shallow depths directly beneath Yantarni Volcano. Instead, magmas of diverse composition are erupted in close succession or are mixed shortly before eruption. We interpret the apparent absence of a shallow chamber with well-developed conduits, together with the small volume of eruptive products, to mean that Yantarni Volcano is in an immature stage of development.

REFERENCES CITED

Aramaki, S., and Yamasaki, M., 1963, Pyroclastic flows in Japan: Bulletin Volcanologique, v. 26, p. 89-99.

Brugman, M.M., and Meier, M.F., 1981, Response of glaciers to the eruptions of Mount St. Helens, in Lipman, P.W., and Mullineaux, D.R., eds., The 1980 eruptions of Mount St. Helens, Washington: U.S. Geological Survey Professional Paper 1250, p. 743-756.

Burk, C.A., 1965, Geology of the Alaska Peninsula--Island arc and continental margin: Geological Society of America Memoir 99, 250 p.

Coats, R.R., 1950, Volcanic activity in the Aleutian arc: U.S. Geological Survey Bulletin 974-B, 49 p.

Conrad, W.K., and Kay, R.W., 1984, Ultramafic and mafic inclusions from Adak Island: Crystallization history, and implications for the nature of primary magmas and crustal evolution in the Aleutian arc: Journal of Petrology, v. 25, p. 88-125.

Detterman, R.L., Miller, T.P., Yount, M.E., and Wilson, F.H., 1981, Geologic Map of the Chignik and Sutwik Island quadrangles, Alaska: U.S. Geological Survey Miscellaneous Investigations Series Map I-1229, 1 sheet, scale 1:250,000.

Detterman, R.L., Case, J.E., Wilson, F.H., Yount, M.E., and Allaway, W.H., Jr., 1983, Generalized geologic map of the Ugashik, Bristol Bay, and part of Karluk quadrangles, Alaska: U.S. Geological Survey Miscellaneous Field Studies Map MF-1539-A, 1 sheet, scale 1:250,000.

Eggler, D.H., 1972, Water-saturated and undersaturated melting relations in a Paricutin andesite and an estimate of water content in the natural magma: Contributions to Mineralogy and Petrology, v. 34, p. 261-271.

Eichelberger, J.C., 1974, Magma contamination within the volcanic pile: Origin of andesite and dacite: Geology, v. 2, p. 29-33.

Ewart, A., Hildreth, W., and Carmichael, I.S.E., 1975, Acid magma in New Zealand: Contributions to Mineralogy and Petrology, v. 51, p. 1-27.

Fisher, M.A., Bruns, T.R., and von Huene, R., 1981, Transverse tectonic boundaries near Kodiak Island, Alaska: Geological Society of America Bulletin v. 92, p. 10-18.

Gill, J.B., 1981, Orogenic andesites and plate tectonics: New York, Springer-Verlag, 390 p.

Hoblitt, R.P., Miller, C.D., and Vallance, J.W., 1981, Origin and stratigraphy of the deposit produced by the May 18 directed blast, in Lipman, P.W., and Mullineaux, D.R., eds., The 1980 eruptions of Mount St. Helens, Washington: U.S. Geological Survey Professional Paper 1250, p. 401-420.

Irvine, T.N., and Baragar, W.R., 1971, A guide to the chemical classification of the common volcanic rocks: Canadian Journal of Earth Sciences, v. 8, p. 523-548.

Kay, R.W., 1978, Aleutian magnesian andesites: Melts from subducted Pacific Ocean crust: Journal of Volcanology and Geothermal Research, v. 4, p. 117-132.

Kay, S.M., Kay, R.W., and Citron, G.P., 1982, Tectonic controls on tholeiitic and calc-alkaline magmatism in the Aleutian arc: Journal of Geophysical Research, v. 87, p. 4051-4072.

Kienle, Juergen, and Swanson, S.E., 1983, Volcanism in the eastern Aleutian arc: Late Quaternary and Holocene centers: Journal of Volcanology and Geothermal Research, v. 17, p. 393-432.

Kuntz, M.A., Rowley, P.D., MacLeod, N.S., Reynolds, R.L., McBroome, L.A., Kaplan, A.M., and Lidke, D.J., 1981, Petrography and particle-size distribution of pyroclastic-flow, ash-cloud, and surge deposits, in Lipman, P.W., and Mullineaux, D.R., eds., The 1980 eruptions of Mount St. Helens, Washington: U.S. Geological Survey Professional Paper 1250, p. 525-540.

Luhr, J.F., and Carmichael, I.S.E., 1980, The Colima volcanic complex, Mexico: Contributions to Mineralogy and Petrology, v. 71, p. 343-372.

Marlow, M.S., Scholl, D.W., Buffington, E.C., and Alpha, T.R., 1973, Tectonic history of the central Aleutian arc: Geological Society of America Bulletin, v. 84, p. 1555-1574.

Marsh, B.D., 1982, The Aleutians, in Thorpe, R.S., ed., Andesites: New York, John Wiley & Sons, p. 99-114.

Miller, T.P., and Smith, R.L., 1977, Spectacular mobility of ash flows around Aniakchak and Fisher calderas, Alaska: Geology, v. 5, p. 173-176.

Miyashiro, A., 1974, Volcanic rock series in island arcs and active continental margins: American Journal of Science, v. 274, p. 321-355.

Moore, J.G., and Sisson, T.W., 1981, Deposits and effects of the May 18 pyroclastic surge, in Lipman, P.W., and Mullineaux, D.R., eds., The 1980 eruptions of Mount St. Helens, Washington: U.S. Geological Survey Professional Paper 1250, p. 421-438.

Papike, J.J., Cameron, K.L., and Baldwin, K., 1974, Amphiboles and pyroxenes: Characterization of other than quadrilateral components and estimates of ferric iron from microprobe data: Abstracts with Programs, Geological Society of America, v. 6, p. 1053-1054.

Peccerillo, A., and Taylor, S.R., 1976, Geochemistry of Eocene calcalkaline volcanic rocks from the Kastamonu area, northern Turkey: Contributions to Mineralogy and Petrology, v. 58, p. 63-81.

Reed, B.L., and Lanphere, M.A., 1972, Generalized geologic map of the Alaska Aleutian Range batholith showing potassium-argon ages of the plutonic rocks: U.S. Geological Survey Miscellaneous Field Studies Map MF-372.

----1973, Alaska-Aleutian Range batholith: Geochronology, chemistry, and relations to circum-Pacific plutonism: Geological Society of America Bulletin, v. 84, p. 2583-2610.

Roeder, R.L., and Emslie, R.F., 1970, Olivine-liquid equilibrium: Contributions to Mineralogy and Petrology, v. 29, p. 275-289.

Rowley, P.D., Kuntz, M.A., and MacLeod, N.S., 1981, Pyroclastic flow deposits, in Lipman, P.W., and Mullineaux, D.R., eds., The 1980 eruptions of Mount St. Helens, Washington: U.S. Geological Survey Professional Paper 1250, p. 489-512.

Sakuyama, M., 1981, Petrological study of the Myoko and Kurohime Volcanoes, Japan: Crystallization sequence and evidence for magma mixing: Journal of Petrology, v. 22, p. 553-583.

Scholl, D.W., Buffington, E.C., and Marlow, M.S., 1975, Plate tectonics and the structural evolution of the Bering Sea region, in Forbes, R.B., ed., Contributions to the geology of the Bering Sea basin and adjacent regions: Geological Society of America Special Paper 151, p. 1-31.

Sheridan, M.F., 1979, Emplacement of pyroclastic flows: A review, in Chapin, C.E., and Elston, W.E., eds., Ash-flow tuffs: Geological Society of America Special Paper 180, p. 125-136.

Siebert, L., 1984, Large volcanic debris avalanches: Characteristics of source areas, deposits, and associated eruptions: Journal of Volcanology and Geothermal Research, v. 22, p. 163-198.

Spear, F.S., and Kimball, K.L., 1984, RECAMP--A Fortran IV program for estimating Fe^{3+} contents in amphiboles: Computers and Geosciences, v. 10, p. 317-325.

Thornton, C.P., and Tuttle, O.F., 1960, Chemistry of igneous rocks, I. Differentiation index: American Journal of Science, v. 258, p. 664-684.

Waitt, R.B., Jr., 1981, Devastating pyroclastic density flow and attendant air fall of May 18--Stratigraphy and sedimentology of deposits, in Lipman, P.W., and Mullineaux, D.R., eds., The 1980 eruptions of Mount St. Helens, Washington: U.S. Geological Survey Professional Paper 1250, p. 489-512.

Walker, G.P.L., 1971, Grain size characteristics of pyroclastic deposits: Journal of Geology, v. 79, p. 696-714.

Williams, H., and McBirney, A., 1979, Volcanology: San Francisco, Freeman Cooper, 391 p.

Wilson, F.H., 1982, Map and tables showing preliminary results of K-Ar age studies in the Ugashik quadrangle, Alaska Peninsula: U.S. Geological Survey Open-File Report 82-140, 1 sheet.

-----1985, The Meshik arc--an Eocene to earliest Miocene magmatic arc on the Alaska Peninsula: Alaska Division of Geological and Geophysical Surveys Professional Report 88, 14 p.

Wilson, F.H., Gaum, W.C., and Herzon, P.L., 1981, Map and tables showing geochronology and whole-rock geochemistry, Chignik and Sutwik Island quadrangles, Alaska: U.S. Geological Survey Miscellaneous Field Studies Map MF-1053-M, 3 sheets.

Wright, J.V., and Walker, G.P.L., 1977, The ignimbrite source problem: significance of a co-ignimbrite lag-fall deposit: Geology, v. 5, p. 729-732.

GPO 785-048/48041